Master Thesis
Department of Civil and Architectural Engineering
Division of Soil and Rock Mechanics

Internal stability of geosynthetic reinforced soil walls

Calculations procedures for practical design

EMIL DAVIDSSON

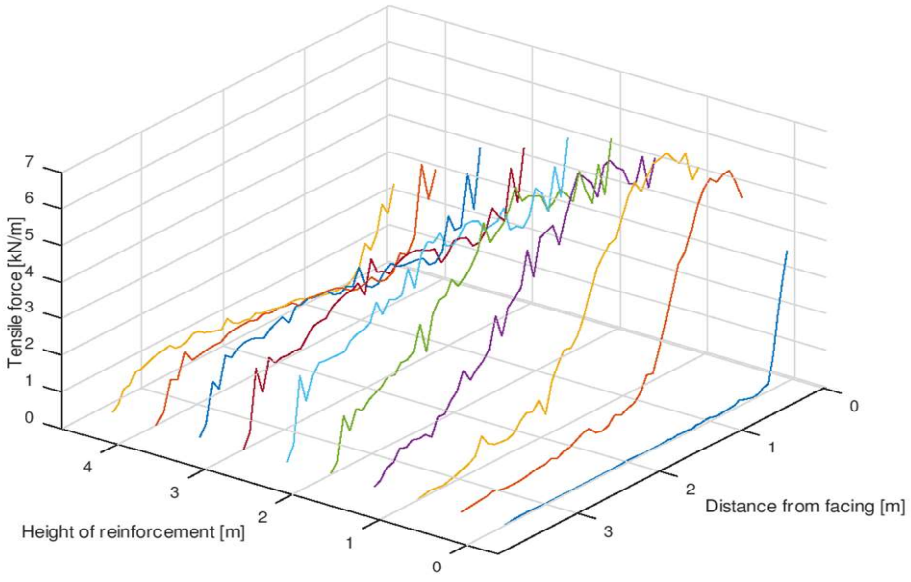

Stockholm, Sverige 2022

Acknowledgements

The author appreciates the support and helpful advice from Stefan Larsson, Fredrik Johansson and William Bjureland at the Department of soil and Rock Mechanics.

Abstract

Reinforced soil constructions have a long history, and various types of the soil reinforcement have been in use since the medieval period. Geosynthetic reinforced soil walls (GRS-walls) while being common throughout the world, in not included in the current Eurocode for geotechnical design, SS-EN 1997-1. The Swedish transportation authority design guidelines (TK Geo 13 and TR Geo 13) provides requirements regarding the utilization of the bearing capacity of the reinforced geosynthetic layer and suggestions for the calculation model, but the design is free to choose a suitable design model. Since geosynthetics are very flexible, the load distribution between the geosynthetic layers in the GRS-wall will be dependent on the stress-strain response of the soil and the geosynthetic layers. This thesis evaluates the importance of the design model on the ultimate limit state (ULS) as well as the serviceability limit state (SLS) on a typical GRS wall. The results shows that a full numerical model including the stress-strain development gives less utilization of the geosynthetic layers at a comparable surcharge load compared to a limit equilibrium model (LEM) suggested by TR Geo. Furthermore, the redistribution of the load between the geosynthetic layers result in a significantly larger maximum load before a collapse state compared to the LEM calculation. In such structures the serviceability conditions will control the design. The consequences for practical design and the limitation to various design models are elaborated and recommendations are given.

Keywords: Geosynthetics, GRS-walls, internal stability

Sammanfattning

Armerad jord har använts naturligt sedan lång tid för att stabilisera jordmassor. Armerad jord med geosynteter, såsom geonät eller geodukar, innefattas inte av den befintliga Eurokoden SS-EN 1997-1. Trafikverkets riktlinjer TK Geo 13 och TR Geo 13 redovisar krav på utnyttjandet av geoynteternas bärförmåga och rekommenderar beräkningsmodell för inre stabilitet, med projektören kan själv välja vilken beräkningsmodell som är lämplig. Eftersom geosynteter är väldigt flexibla kommer lastfördelningen i armerad jord till stor del bero på spännings-töjningssambandet mellan jorden och geosynteternas när konstruktionen påverkas av en last. Detta examensarbete behandlas beräkningsmodellen för inre stabilitet för armerad jord, både för brottgränstillstånd och för bruksgränstillstånd. Resultaten visar att en numerisk modell som innefattar spännings-töjningsberoendet för jorden och geosynteter ger mindre utnyttjande av geosynteternas bärförmåga jämfört med en traditionell brottgränsmodell. Omfördelningen av lasten mellan lagren av geosynteter i den armerade jorden gör också att den numeriska modellen kan nå en betydligt högre yttre last innan konstruktionen fallerar. I ett sådant fall kommer bruksgränstillståndet ha stor vikt för den tillåtna lasten. Påverkan på projektering av armerad jord och begränsningar för olika beräkningsmodeller diskuteras och avslutningsvis ges några rekommendationer för projektering.

Nyckelord: Geosynteter, armerad jord, inre stabilitet

List of symbols

Greek symbol	Explanation	Unit
ε_r	Tensile strain of reinforcement	[-]
γ	Self-weight of soil	
σ_0	Lateral earth pressure of soil at rest	[kN/m²]
σ_h	Horizontal stress	[kN/m²]
σ'_h	Effective horizontal stress	[kN/m²]
σ_a	Active earth pressure	[kN/m²]
σ'_v	Effective vertical stress	[kN/m²]
σ_v	Total vertical stress	[kN/m²]
φ	Internal friction angle	[degree]

Latin symbol	Explanation	Unit
EA	Tensile stiffness	[kN/m²]
EI	Flexural rigidity	
c	Cohesion	[kN/m²]
G	Force from self-weight of soil wedge	[kN/m²]
H	Total height of GRS-wall	[m]
h	Height of geosynthetic reinforcement level	[m]
K	Earth pressure coefficient	[-]
K_a	Active earth pressure coefficient	[-]
K_0	Earth pressure at rest coefficient	[-]
L	Length of geosynthetic reinforcement	[m]
L_e	Pull-out length of reinforcement	[m]
L_r	Length of reinforcement inside Rankine wedge	[m]

M	Degree of mobilization of reinforcement	[m]
P_{a}	Active earth pressure resultant	[kN/m]
T_{mob}	Mobilized tensile force	[kN/m]
T_{req}	Required tensile strength of reinforcement as calculated by with SGF (2004)	[kN/m]
T_{ult}	Ultimate tensile strength of reinforcment	[kN/m]
q	Surcharge load	[kN/m²]

Contents

1 Introduction

Reinforcing soil is a technique whereby a soil body is layered with another material to increase the strength and stability of the soil body. The technique of reinforcing soil with wood dates back to the 16th century (Holtz, 2017).The first modern method for reinforcing soil with was invented by the French engineer Henri Vidal in the 1960's. Since then, reinforcing soil with steel or geosynthetic mats or strips has become increasingly popular. Today the estimate is that there is 100,000 or more geosynthetic reinforced soil walls around the world (Koerner, 2017). Geosynthetic Reinforced Soil Walls, hereafter abbreviated GRS-walls, have been used for a variety of different applications such as bridge abutments, road embankments and retaining walls. They have also been used in specialized applications such as bridge abutments for high-speed railways in Japan and walls and steep slopes as high as 74 m. A review of many structures have shown that building the aforementioned structures as GRS-walls results in lower construction costs in comparison to cantilever and gravity walls (Koerner & Song, 2001). It is however important to note that Geosynthetic Reinforced Soil walls are not a suitable replacement for soil retaining structures used for excavations, such as sheet pile walls or soil nailing as it cannot be utilized to reinforce soil in-place.

1.1 Background to the study

The design of GRS-walls is not addressed in the geotechnical section of the Eurocodes. Some countries have introduced national codes for design, e.g. the British Standard (BSI, 1995), the German Standard (German Geotechnical Society, 2011), and the Norwegian standard for road construction (Statens Vegvesen, 2005). A Nordic guideline has been published which presents suggestions for the design of Geosynthetic reinforced walls, (SGF, 2004). The calculcation methods presents there is suggested in the Swedish road authority guidelines TR Geo 13 (Trafikverket, 2014). The Nordic Guideline s a cooperation between the Swedish Geotechnical Society and the Norwegian, Danish and Finnish societies for Soil Mechanics and Foundation Engineering. . This guideline is however no standard or national code, but recommendations for design. The area is consequently unregulated, and design in Sweden has been carried out following the Nordic Guidelines, but also according to the German guidelines. The trend in large-scale projects in Sweden is that companies from other countries such as Germany, Switzerland, Austria, and Italy are managing large design-and-build contracts. The design of Geosynthetic Reinforced Soil walls can therefore be designed in e.g. Germany, and local technical auditors need to assess the design relative to foreign national codes. The legal basis for acceptance or refusal of design is therefore based on the codes of another country, and more knowledge about the practical consequences of design is desirable to assess the design.

A previous study comparing the Nordic Guidelines for Reinforced Soil and Fill (SGF, 2004) with the guidelines of the Norwegian transport agency (Statens Vegvesen, 2005) and the British Standard (BSI, 1995) was carried out in Bendzovski & Melin (2007). It found that that SGF (2004) were hard to follow and lacking in accommodating different loading conditions and complex geometries (Bendzovski & Melin, 2007). A survey about the use of reinforced soil in Sweden found that lacking experience with such structures was one of the most important factors to why they are not utilized in projects (SGF, 2005). Lack of experience and a rudimentary design guideline would naturally be obstacles when it comes to designing any structure. Geological conditions could of course also play a role in favoring other types of structures, but as experience and research have shown geosynthetic reinforced soil walls can be adapted to almost any type of fill material, including fills with clay content (Koerner, 2017).

The most important aspect of the structural behaviour of a geosynthetic reinforced soil wall is how the horizontal earth pressure of the soil is transferred to the geosynthetic reinforcements. This dictates the required strength of the geosynthetic reinforcements. The assumption made in the SGF (2004) is that the strain of the soil and geosynthetic reinforcements are large enough to enable active earth pressure conditions. Each layer of geosynthetic reinforcement is assumed to counter the load applied by the horizontal earth pressure at the level of each reinforcement. This assumption ignores the potential

redistribution of load between the reinforcement layers. Redistribution of the load results in a significantly higher load-carrying capacity of the GRS-wall. Understanding the mechanical behaviour GRS-walls is of importance to understand potential limitation of the design method.

1.2 Objective of the current study

The aim of this thesis is to evaluate the current limit equilibrium model for internal stability of GRS-wall in comparison to a numerical model including load-distribution between reinforcement layers in a numerical model incorporating the stress-strain response of the geosynthetic material and the soil. Since both types of calculation models are allowed in practical design, the resulting necessary reinforcement for a GRS-wall could be very different. The difference between the models in both the Ultimate Limit State (ULS) and Serviceability Limit State (SLS) are evaluated. Based on the conclusions recommendations for practical design are given.

1.3 Outline of thesis

A numerical model of a geosynthetic reinforced soil wall is created in FEM-software Plaxis 2D to determine the earth pressure conditions, reinforcements strains and mobilized loads in the geosynthetic reinforcements including the load distribution between the reinforcement layers. This choice was made since field and laboratory experiments have previously been carried out with GRS-walls and were considered too cumbersome of the current study. SGF (2004) is used to determine the minimum required tensile strength for the reinforcements for two GRS-walls with different reinforcement spacing width at the onset of collapse by tensile over-stress in the reinforcements. These values are then used as input value in numerical models. In addition, a loading test is performed on both these modelled GRS-walls, as well as FEM calculations using reinforcements of lower strength than the required minimum tensile strength value from SGF (2004). The aim of the method is to investigate the structural behavior of GRS-walls at the assumed ultimate limit state in SGF (2004) and at the simulated onset of collapse.

1.4 Limitations

The study is limited by the ability of the numerical model to produce realistic representations of reality. The model represents a validation of the design idealization, but not a verification, which requires experimental evidence. The possible systematic errors of the numerical model therefore influence the results. The geosynthetic reinforcement is modelled as an elastic-perfectly plastic material and does not take the non-linear stress-strain-time response into account, which is a significant limitation. The scope of the study is limited to the failure by tensile overstress of the geo synthetic reinforcements, other failure modes are accounted for in the numerical modelling, but not explicitly studied in this thesis.

2 Geosynthetic reinforced walls

2.1 Introduction

This chapter contains an overview over the basic principles of GRS- walls some design idealizations, and geomechanical theory relevant to the study.

2.2 Geosynthetic Reinforced Soil Walls

2.2.1 Construction of GRS-walls

The construction of a GRS-wall is carried out bottom-up. In the first stage of construction the site is prepared by levelling the ground at where the bottom reinforcement layer is then then placed. This means that if the GRS-wall is supposed to replace an existing slope, the slope has to be excavated prior to the construction. The first reinforcement layer is then placed on the subsoil or foundation and then a layer of fill is placed on top and compacted before the next reinforcement layer is placed on top. This procedure is then repeated until the desired height of the wall is reached. A schematic view of a GRS-wall can be seen in Figure **1** below.

2.2.2 Applications

GRS-walls can be used for different applications such as retaining walls, steep slopes, bridge abutments and sound barriers (SGF, 2004). Examples of such structures can be seen in Figure 2 GRS-walls are applicable when the ground level should be expanded relative to the original ground level or when excavation before construction is possible.

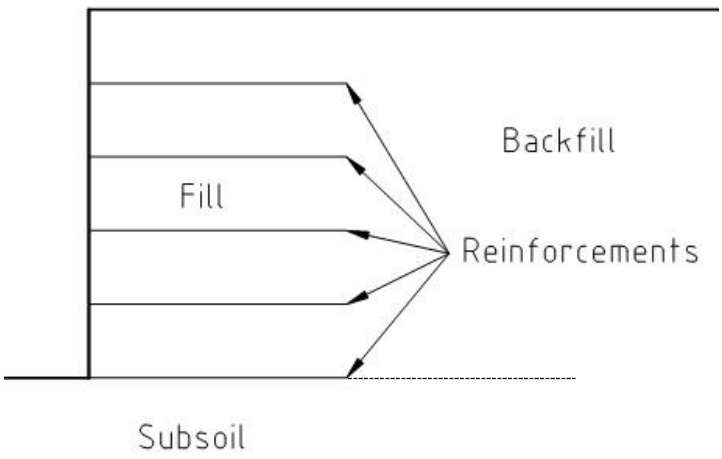

Figure 1 Schematic overview of GRS-wall

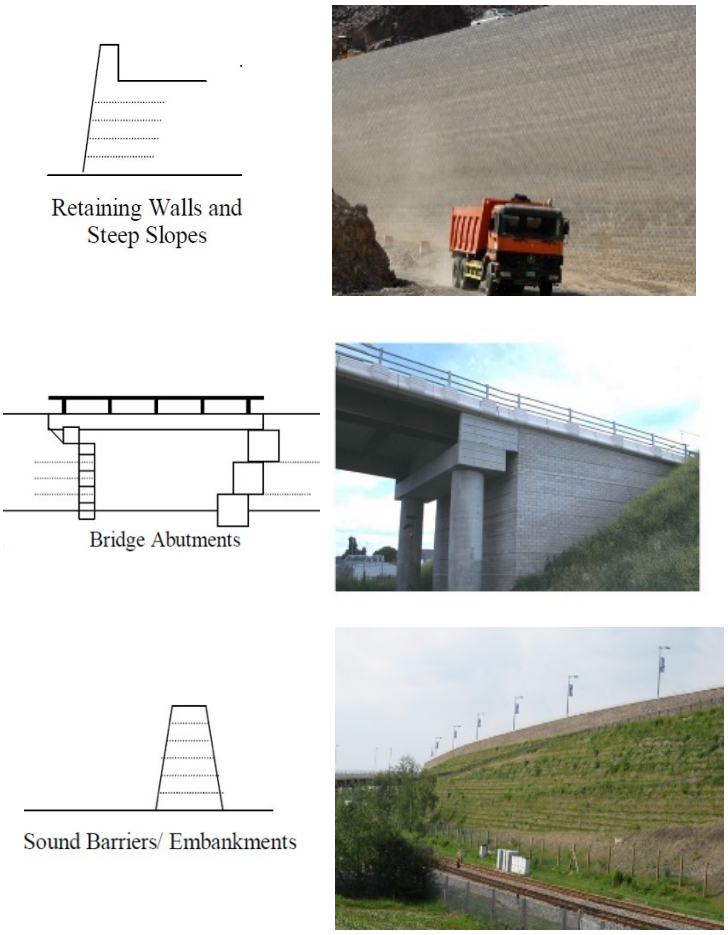

Figure 2 Examples of applications for GRS-structures shown in pictures and schematically, Insert pictures are shown with permission from Tensar Ltd.

2.3 Failure modes of GRS-walls

In Figure **3** an overview of possible failure modes of GRS-structure is presented (Bathurst & Simac, 1994). Depending on the geometrical configuration of the structure, reinforcement strength, facing, reinforcement-facing connection, fill material, and subsoil, the different failure modes are more or less likely to occur. It is therefore important to be aware of all aspects of the structure in design.

Failure modes are often divided into internal and external or global failures, such as in SGF (2004). Internal failures meaning failures occurring inside the reinforced zone and external failures being failures circumventing the structure, i.e. outside the reinforced soil zone. Main focus of this study e) tensile over-stress as depicted in Figure **3**.

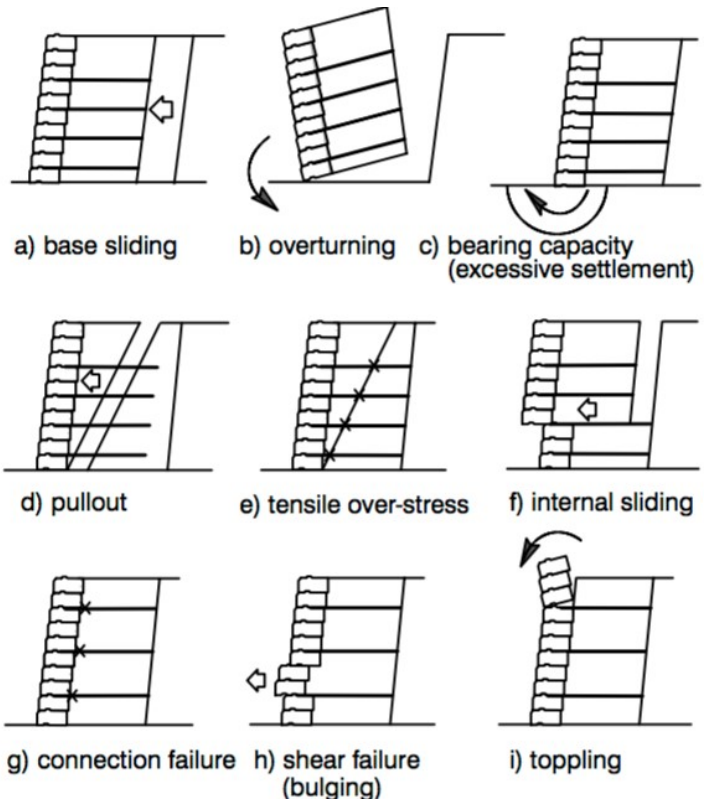

Figure 3 Failure modes of a GRS-wall (Bathurst & Simac, 1994)

2.4 Geosynthetic reinforcement

Geosynthetic reinforcements are made from linear polymer elements which can be combined in different ways. The different types can roughly be divided in to the following categories (Jewell, 1996).

- *Geogrids*: created through heating and stretching a polymer sheet or combining strips or yarns in two perpendicular directions with joints at the intersections.
- *Woven*: made up from two perpendicular sets of parallel linear elements which are intertwined to form a planar fabric
- *Non-woven*: made up from randomly arranged filaments which are bonded together mechanically, thermally or chemically.
- *Strips*: made up from parallel yarns which are fixed and protected by a polymer coating

The geosynthetic reinforcements can be made up from different types of polymers, such as polyester, polypropylene and polyethelene. The most important difference between the materials is the force-strain behaviour. The force-strain behaviour determines the developed strain in the material under a given asserted force. In Figure 4, force-strain behaviour is shown for a selection of polymeric materials and other materials. Polymers exhibit much larger strains for any given force, in comparison to other reinforcement materials such as steel. This is important as it affects the soil-reinforcement interaction.

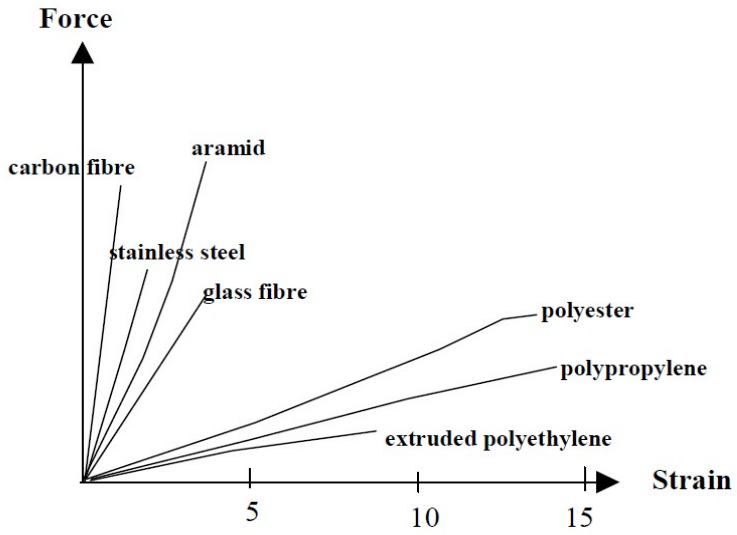

Figure 4 Typical force-strain behaviour for different materials (Carlsson, 1987)

The purpose of geosynthetics as soil reinforcement is to alter the force equilibrium of a soil body by providing internal tensile resistance and thus improving the shear resistance of the structure (SGF, 2004). The resistance originates from the force mobilized as tensile strain in the reinforcement and soil develops (Jewell, 1996). The largest strains in the soil body occurs in the shear failure zone and thus will the largest tensile forces in the reinforcement occur at the intersection of the shear surface, as is shown in Figure **5**. This means that the structure is internally supported as the force in reinforcement is mobilized locally at the shear zone (Wu, 2007)

The mobilisation of tensile force in the reinforcement occurs through the bond stress between soil and reinforcement (Hoffman, 2015). The mobilization of bond stress occurs through frictional contact between the soil particles and the reinforcement surface and from bearing stresses on the transversal members of the reinforcement in case of geogrid-reinforcement (SGF, 2004).

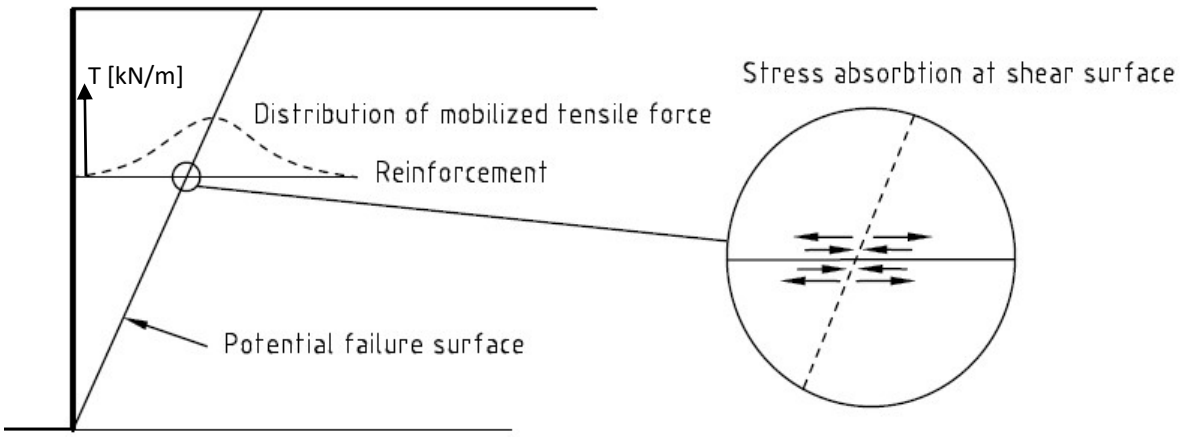

Figure 5 Mobilized tensile force in reinforcement and stress absorption at shear surface (SGF, 2004)

To explain this, consider a soil body which is vertically loaded. The load causes compressive strain in the vertical direction and tensile strain in the horizontal direction. If a horizontally oriented reinforcement is introduced to the soil body, the horizontal strain will induce shear forces at the soil-reinforcement interface. This shear force is the bond stress between the soil and the reinforcement (Hoffman, 2015). In the case of a wall or steep slope the directions of principal strain are not aligned in the horizontal and vertical direction. Reinforcements are, however, preferably installed horizontally regardless as to not design structures which are impractical to build (Shukla, et al., 2011).

2.5 Facing of GRS-walls

To prevent the soil from falling out at the face of the wall, a facing element is attached to the end of the reinforcement, or the reinforcement is wrapped around the soil layer. There exist several different facing types, but mechanically they can be sorted into three categories with regard to flexural stiffness (Nordic Geosynthetic Group, 2005).

- Stiff– completely rigid facing with no capability to accommodate differential lateral settlements, i.e. precast full height concrete facing
- Flexible/partially deformable facing – stiff blocks which can accommodate differential settlements between the blocks which make up the facing, i.e modular concrete block walls.
- Soft/deformable facing elements – facing without flexural stiffness where the soil is retained by the geosynthetic reinforcement, i.e. wraparound.

In Figure 6 examples of different facing types are shown.

Its been shown in case studies that the effect of facing stiffness and toe restraint is significant in determining how much load is carried by the reinforcements (Allen & Bathurst, 2002). The stiffer the facing is, the more load is carried by the facing and the less load is carried by the reinforcements. This is due to that a stiffer facing does not let the soil translate outwards freely, the facing must then carry more load. This is a general mechanical trait, stiffer elements in a structure carry a higher degree of the load than less stiff elements.

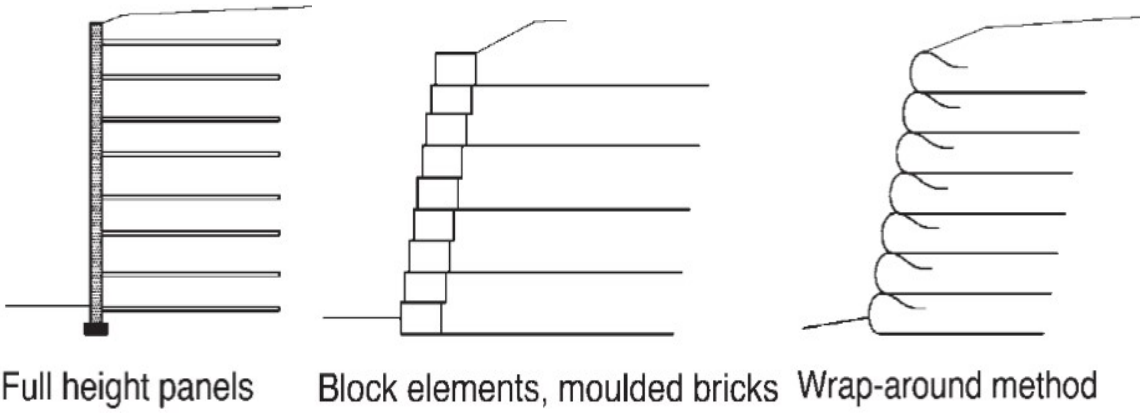

Figure 6 Three types of facing configuration with different stiffness (German Geotechnical Society, 2011)

2.6 Design codes and guidelines

In many countries design codes and guidelines have been put forward by different agencies, in some countries such as the USA multiple guidelines from different associations and agencies exist in parallel (Zornberg & Leshchinsky, 2003). The design of GRS-walls is unregulated in the Eurocode 7 (SS-EN 1997-1), but some countries like Great Britain and Germany have put forward national standards. There is no national standard in Sweden but the Nordic Guidelines for Reinforced Soil and Fill (SGF, 2004) contains a design method for GRS-walls, which is recommended in the Swedish transportation authority guidelines TR Geo 13 (Trafikverket, 2014).

Many of design codes and guidelines have adopted a design approach based on the mobilization of active earth pressure as calculated with Rankine's earth pressure theory (Zornberg & Leshchinsky, 2003). This is also the case for SGF (2004), the design method from this guideline is presented in detail in chapter 3.

2.7 Strain compatibility of reinforcement and soil

However, the Nordic guideline is simplified in many respects, especially regarding the load distribution for the reinforcement layers, which is a result of the strain compatability. The strain compatability determines the relation between the developed shearing resistance of the soil and the mobilized tensile force in the reinforcement for a given horizontal strain. Both the tensile strength of the geosynthetic reinforcement and the internal friction angle are mobilized by tensile strain. If we consider a case where a soil body reinforced with a geosynthetic is at first held in place by an imaginary horizontal force, the horizontal strains are zero and the soil is at rest. Removing this imaginary force will allow for the soil to deform horisontally, which induces strains in the soil and reinforcement. The mobilization of shearing resistance and the tensile force in the reinforcement is shown schematically in Figure 7.

The mobilized friction angle in a dilatant soil, φ'_{mob}, increases up to a certain level of strain after which it decreases, meaning that the required force to hold the structure in equilibrium will decrease up to the point of the peak friction angle φ'_p after which it increases as the soil moves toward the residual friction angle φ'_c. The available force to hold the structure in equilibrium, i.e. the mobilized tensile force in the reinforcement, will increase with the strain up to the point where the reinforcement reaches its plastic limit. The two behaviours can be combined in a strain compatibility diagram where the expected equilibrium between the soil and reinforcement response is at the intersection of the available and required force as seen in Figure 8.

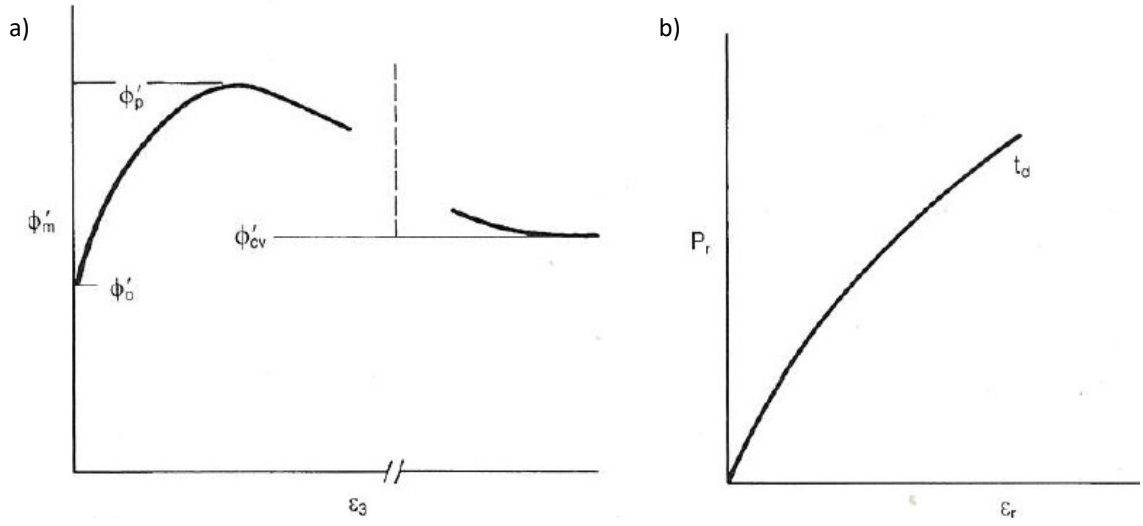

Figure 7 a) Mobilization of friction angle. The schematic figure is not continuous to reduce the length of the figure. b) Mobilization of tensile force in reinforcement (Jewell, 1996)

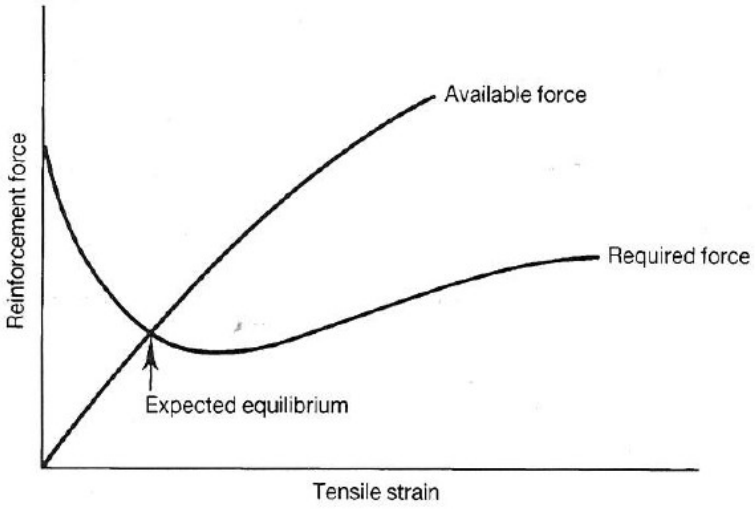

Figure 8 Strain compatability diagram **(Jewell, 1996)**

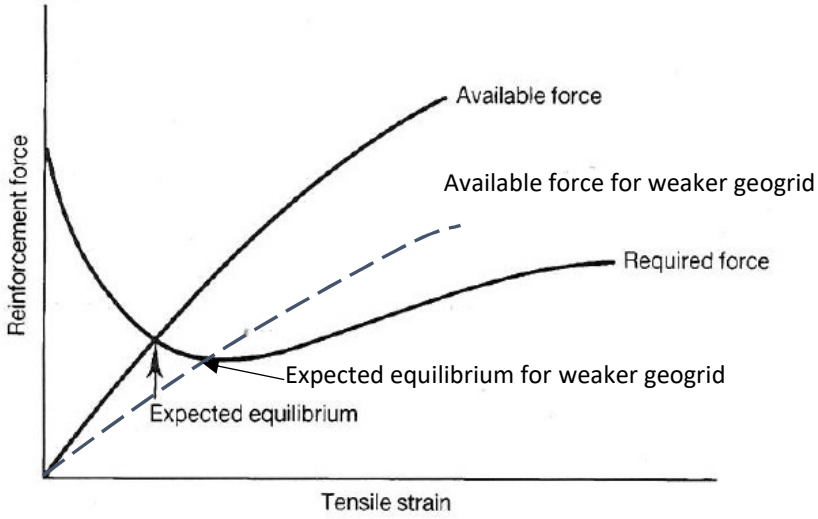

Figure 9 Strain compatability diagram **(Jewell, 1996)** for two different geosynthetic reinforcements. Force-strain response shown by the dashed line is added by the author.

To show how the expected equilibrium is affected using a reinforcement with different force-strain response, a force-strain response curve of a more flexible geosynthetic reinforcement is added in Figure 9. As can be seen in the figure a weaker reinforcement will shift the equilibrium, in this case close to the peak friction angle. The mobilized force in the reinforcement will in this instance be lower but occur at a higher level of strain.

2.8 Load redistribution effect

Conventional design, i.e. Rankine based methods, does not take into account potential load redistribution effects in the GRS-wall. Physical models of GRS-walls tested in centrifuge tests showed a load distribution of tensile forces that varied due to the mobilization of tensile force in the reinforcements (Zornberg, et al., 1998). As a reinforcement level is close to reach yield, load is distributed to nearby reinforcements, thus creating a ductile behaviour of the structure. A schematic view of the distribution is shown in Figure 10.

For load redistribution to be effective, the structural members must be able to elongate longer than the local yield criteria of the surrounding material without breaking (Chen, 1997). As the soil is stiffer than

the of the geosynthetic reinforcement, the geosynthetic reinforcements can elongate longer than the yield criteria of the soil and redistribute loads to nearby reinforcement layers.

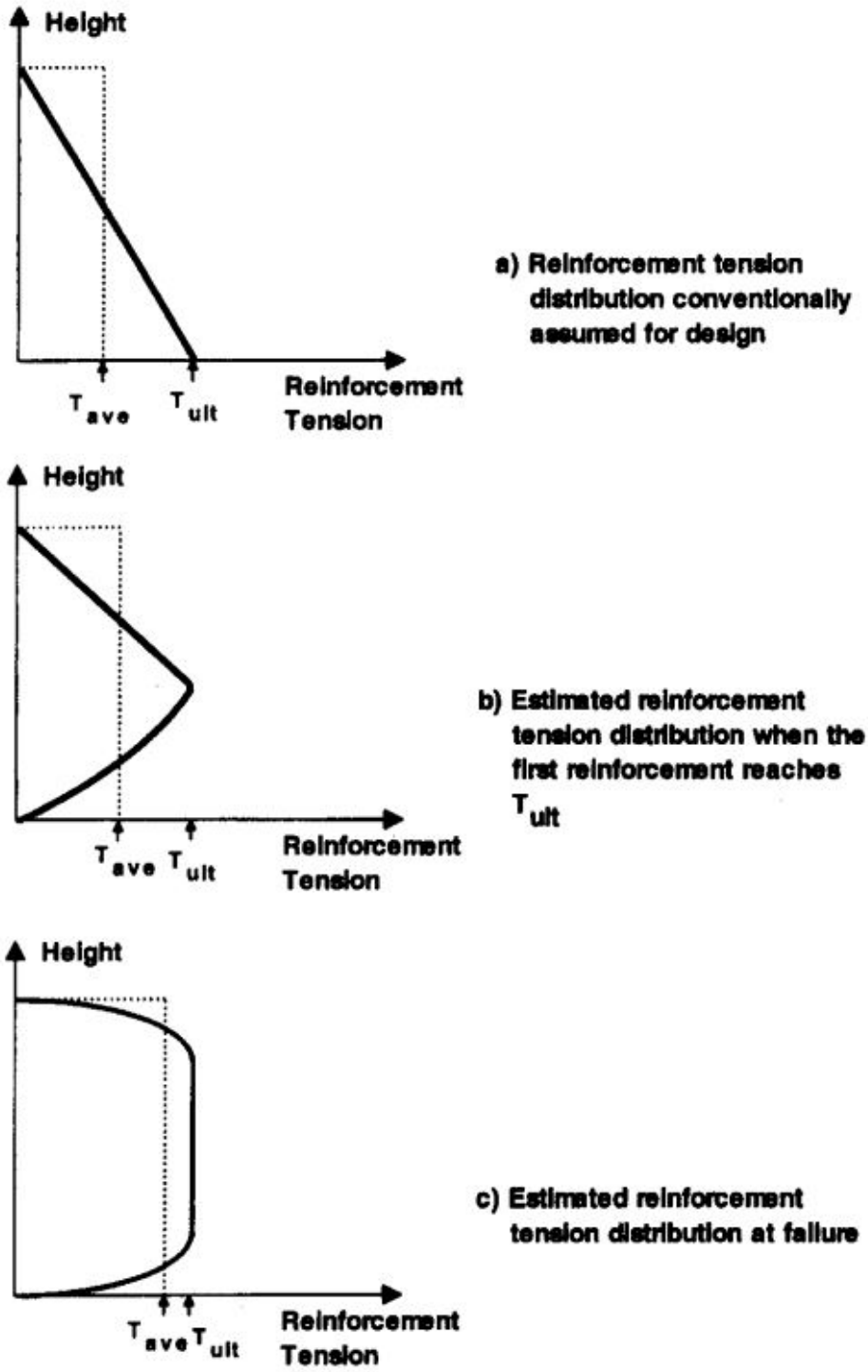

Figure 10 Load distribution in a GRS-wall under varying degrees of mobilization of geosynthetic reinforcements **(Zornberg, et al., 1998)**

3 Methodology

The current chapter explores the earth-pressure theory which forms the background to the Nordic guidelines. The numerical model is then presented. A comparative study between the Nordic guidelines and the numerical models is then presented, and a parameter study carried out with the numerical model. The comparative study is based on the limit state for tensile overstress of SGF (2004) in which one of the reinforcement layers reach yield in the absence of safety factor.

3.1 Earth pressure theory

The design in SGF (2004) is done according to Rankine's theory of active earth pressure presented in this chapter.

3.1.1 Rankine's earth pressure theory

The load applied on the GRS-structure, which must be resisted by the reinforcements, originates from the horizontal earth pressure. Plasticity theory states that the magnitude of the horizontal earth pressure is dependent on the horizontal strain. According to Rankine's theory of earth pressure the horizontal earth pressure is formulated as (Rankine, 1857):

$$\sigma_h = K * \sigma_v \tag{1}$$

Where σ_v is the vertical earth pressure and K is a horizontal earth pressure coefficient. As K is dependent on strain it will differ depending on the deformations of the soil. The active earth pressure coefficient, K_a , and the passive earth pressure coefficient, K_p represent the states of plastic equilibrium in Rankine's earth pressure theory while K_o represents the elastic equilibrium for soil at rest. A schematic view over the horizontal earth pressure coeffients relation to soil deformation is shown in Figure 11.

Active earth pressure conditions occur when a soil retaining structure is pushed away by the retaining soil. The tensile deformation in the soil relieves stress leading to a horizontal earth pressure which is lower than the at rest earth pressure. Conversely if the retaining structure pushes on the soil body passive earth pressure conditions occur. As the soil is compressed additional horizontal stress occurs in the soil body. The active and passive state represent the theoretical minimum and maximum of horizontal earth pressure (Terzaghi & Peck, 1948).

As tensile strains are needed to mobilize the geosynthetic reinforcements Rankine's active earth pressure is often used to determine the loads exerted on a GRS-wall. Figure 12 shows active, passive, and at rest earth pressure distribution.

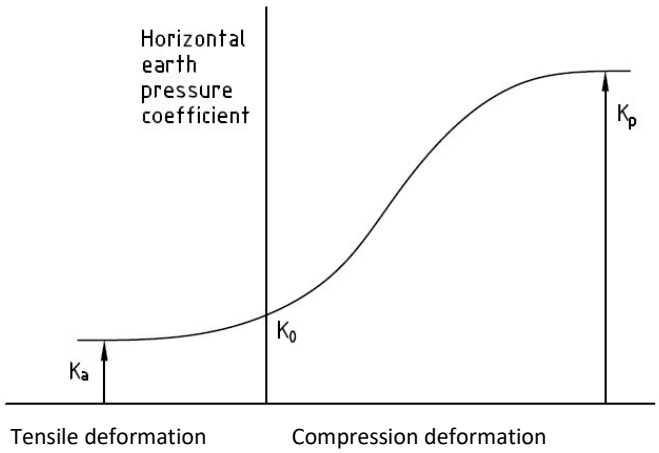

Figure 11 Schematic view over the horizontal earth pressure coefficients relation to soil deformation.

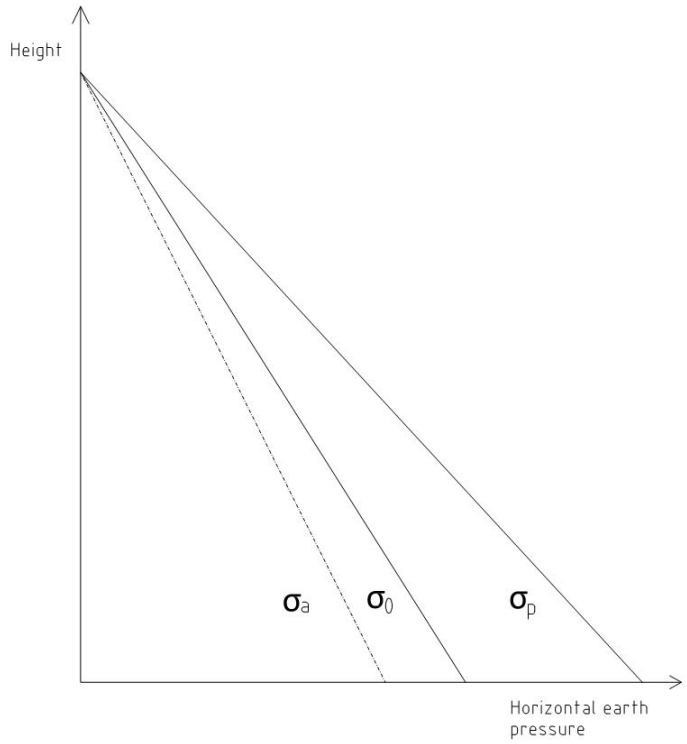

Figure 12 Schematic figure of the active, at-rest and passive earth pressure distribution

For the case of frictional soil without cohesion the active earth pressure σ'_a can be expressed as (Terzaghi & Peck, 1948).

$$\sigma_a = \sigma'_v K_a + u \quad (2)$$

Where

$$K_a = tan^2(45 - \frac{\varphi}{2}) \quad (03)$$

The passive earth pressure can be expressed as (Terzaghi & Peck, 1948)

$$\sigma_p = \sigma'_v K_p + u \quad (04)$$

Where

$$K_p = tan^2(45 + \frac{\varphi}{2}) \quad (5)$$

The earth pressure at rest for a normally consolidated soil can be expressed as (Jaky, 1948)

$$\sigma'_0 = \sigma'_v K_0 \quad (6)$$

Where

$$K_0 = 1 - sin\ \varphi \quad (7)$$

3.1.2 Calculation of design loads in SGF (2004)

As active earth pressure conditions are assumed loads are calculated with eq. (2) and (03).

Where

$$\varphi_d = \arctan(\frac{\tan(\varphi_k)}{\gamma_\phi}) \quad (8)$$

φ_d is the design friction angle, φ_k is the characteristic value of the friction angle and γ_ϕ is the partial coefficient of the friction angle.

The vertical effective stress $\sigma'_{v,d}$ is calculated as:

$$\sigma'_{v,d} = \sigma_{v,d} - u \quad (9)$$

Where

$$\sigma_{v,d} = \gamma_d h + q_d \quad (10)$$

$$u = \gamma_{wd} h_w \quad (11)$$

$\sigma_{v,d}$ is the design total stress, $\sigma_{v,d}$ is the design unit weight of the soil, h is the depth to a given level in the structure, q_d is the design surcharge, u is the pore water pressure, γ_{wd} is the unit weight of water and h_w is the depth below the water table at a given level in the structure.

3.2 Design according to SGF (2004)

In this section limitations regarding geometry and loading conditions, calculation of loads and design. The design of GRS-walls in SGF (2004) is only specified with regard to the internal failure modes pull out and tensile over-stress and the external failure mode of basal sliding. For other possible failure modes SGF (2004) refers to conventional design methods. This calculation method is also suggested in TR Geo 13.

3.2.1 Geometry and loading limitations

The potential internal failure is therefore assumed to occur at an angle of 45+fi/2 degrees to the horizontal plane. The design method is only suited for GRS-walls with face inclination β between 80-90 degrees to the horizontal and an evenly distributed surcharge or no surcharge.

The geometrical parameters of the GRS-wall are the vertical spacing, S_v, between the reinforcement layers, height of the wall, H, and length of the reinforcements, L. Any effect of face inclination is neglected in the design (SGF, 2004).

3.2.2 Internal failure modes

3.2.2.1 Design strength tensile strength of reinforcement

The design value of the tensile strength T_d is derived from the horizontal earth pressure as shown in Figure 13. If S_v and T_d are constant through the wall the largest earth pressure resultant will occur at the bottom as the earth pressure increases with depth. The required value of T_d, for each reinforcement level is calculated as:

$$T_\mathrm{d} \geq S_\mathrm{v} * p_{\mathrm{a,d,max}} \tag{12}$$

Typically the unfactored characteristic tensile strength T_k is given by the manufacturers. To find a suitable reinforcement, T_d can be derived from T_k by accounting for the partial coefficients used to account for creep, installation damage, chemical and biological degradation of the reinforcement as:

$$T_\mathrm{d} = \frac{T_\mathrm{k}}{\eta_1 * \eta_2 * \eta_3} * \gamma_\mathrm{m}, \tag{13}$$

Where η_1 is the creep factor of the material, $\eta_2$is the installation damage factor dependent on fill material and η_3 is the chemical and biological degradation factor. γ_m is the reinforcement partial factor.

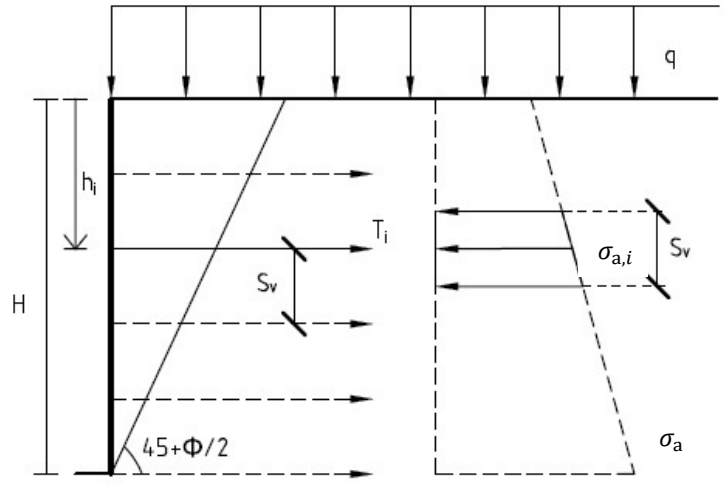

Figure 13 Acting forces on a given reinforcement layer in accordance with Rankin's active earth pressure (Jewell, 1996).

3.2.2.2 Pull-out length

Pull-out is defined as the minimum length of reinforcement required behind the Rankine wedge to achieve sufficient bond stress, as shown in Figure 14. The pull-out length is denoted L_e and is calculated as:

$$L_e \geq \frac{0.5 * \sigma_{a,d} * S_v}{\frac{\alpha_1}{\gamma_p}(c'_d + \gamma_d * h * \tan(\varphi_d))} \tag{14}$$

Where γ_p is the partial factor with regard to pull-out and α_1 is the reinforcement-soil bond coefficient.

L_e is recommended to have a value of minimum of 1 m independent of the calculations.

Trigonometry is used to calculate the total required reinforcement length. L_r denotes the length of the reinforcement inside the soil wedge and is calculated as:

$$L_r = (H - h)\tan\left(45 - \frac{\varphi_d}{2}\right) \tag{15}$$

The total reinforcement length is then given as:

$$L = L_e + L_r \tag{16}$$

In general values sufficient values of L are between $0.6H$ and $0.8H$ (SGF, 2004).

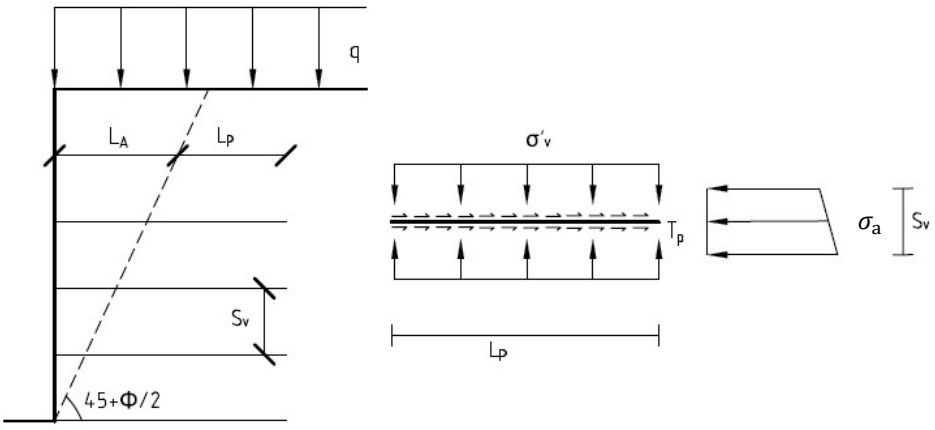

Figure 14 Design against failure by pull-out (Jewell, 1996)

3.2.3 Calculations for comparison with the numerical model

The same geometrical and soil parameters as used in the numerical models are used to calculate a minimum required tensile strength, denoted T_{req}, for each reinforcement level. The highest value out of all reinforcement levels is considered governing and is denoted $T_{\mathrm{req,gov}}$. All input values are unfactored as to simulate a GRS-wall at the limit of tensile overstress for SGF (2004).

3.3 Numerical model including the stress-strain behaviour in a finite element framework

This chapter first introduces geometrical conditions then material model and finally the calculation sequences performed.

3.3.1 Geometry

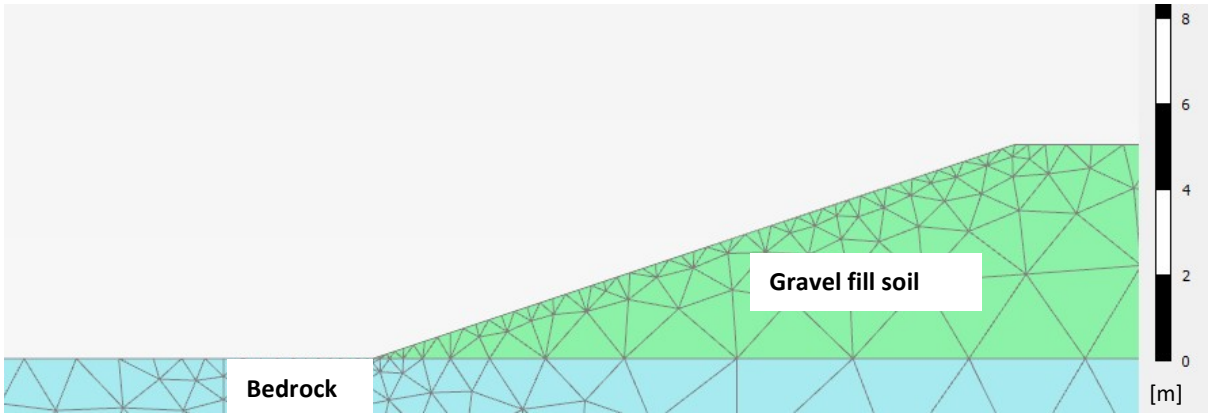

Figur 15 Initial conditions for Plaxis 2d model

The initial conditions before the GRS-wall is modelled is shown in Figur 15.The foundation at which the GRS-wall is placed is modelled as homogenous bed rock and the soil behind the GRS-wall is a gravel fill soil. The surface of the bedrock is horizontal, and the fill soil is a 5 m high slope on top of the bedrock.

The geometry of the GRS-wall at the end of construction is shown in table 1. Calculations are performed for a few different scenarios as shown below, the only variable geometrical parameter in this study however is S_v.

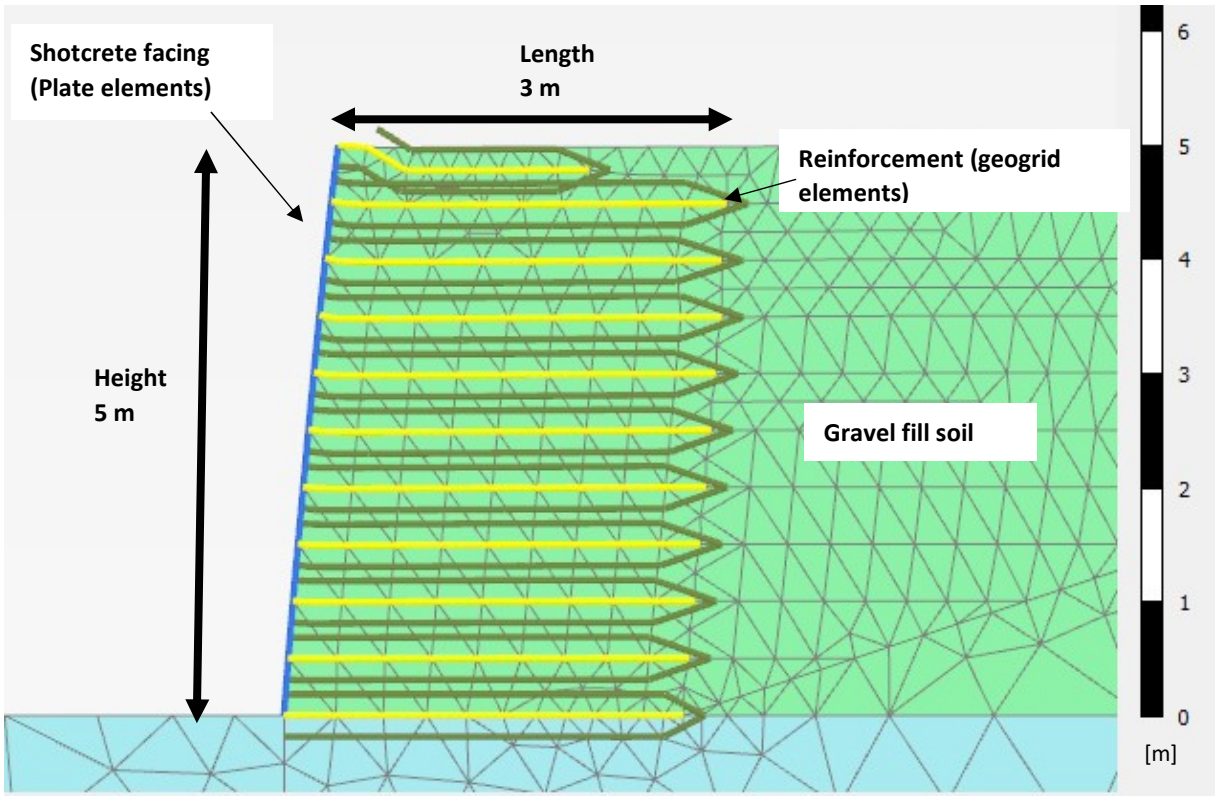

Figure 16 Geometry and materials at end of construction

Table 1 Geometry of GRS-wall

H[m]	L[m]	Facing Inclination	$S_v[m]$
5.0	3.0	10:1	0.5 / 1,0

3.3.2 Material models

3.3.2.1 Fill soil

The fill soil is modelled as a gravel with the Mohr-Coulomb constitutive soil model. The same fill soil is used both in and behind the reinforced zone. Parameters are shown in table 2.

Table 2 Properties of fill soil (gravel)

Parameter	Name	Value	Unit
Material model	Model	Mohr-Coulomb	-
Type of material behaviour	Type	Drained	-
Soil unit weight above phreatic level	γ	19	[kN/m³]
Young's modulus (constant)	E'	25000	[kN/m²]

Poisson's ratio	ν'	0.29	-
Cohesion	c	0	[kN/m²]
Friction angle	φ'	37	[deg]
Dilatancy angle	ψ	7	[deg]
Interface parameter	R_{inter}	0.8	-

3.3.2.2 Bedrock

The foundation for the GRS-wall is modelled as bedrock with parameters as listed in table 3.

Table 3 Properties of subsoil material (bedrock).

Parameter	Name	Value	Unit
Material model	Model	Linear-elastic	-
Soil unit weight above phreatic level	γ	27	[kN/m³]
Young's modulus (constant)	E'	$50*10^6$	[kN/m²]
Poisson's ratio	ν'	0	-

3.3.2.3 Geosynthetic reinforcement

The geosynthetic reinforcement is modelled with geogrid elements. The stiffness of the reinforcements is set to have the same relative stiffness in relation to the ultimate strength as Huesker Fortrac 35T (NorGeoSpec, 2017), the stress-strain curve for Huesker Fortrac is shown in Figure 17. As Plaxis only allows a linear stiffness model, *EA*, is modelled as the secant stiffness at 2% strain. The relation between *EA* and T_{ult} is shown in eq. (17).

$$EA = T_{ult} * 12.5 \quad (17)$$

Four geosynthetic reinforcements of different strengths are utilized for the modelling. Three for calculations with $S_v = 0{,}5\ m$ and one for $S_v = 0{,}5\ m$. As shown in table 4.

Table 4 Properties of geogrids (geosynthetic reinforcement)

Parameter	Name	Value	Unit
Material model	Model	Elastic-plastic	-
Normal stiffness ($T_{ult} * 12.5$)	EA	62.5, 100, 137.5, 237.5	[kN/m]
Tensile strength	T_{ult}	5, 8, 11, 19	[kN/m]

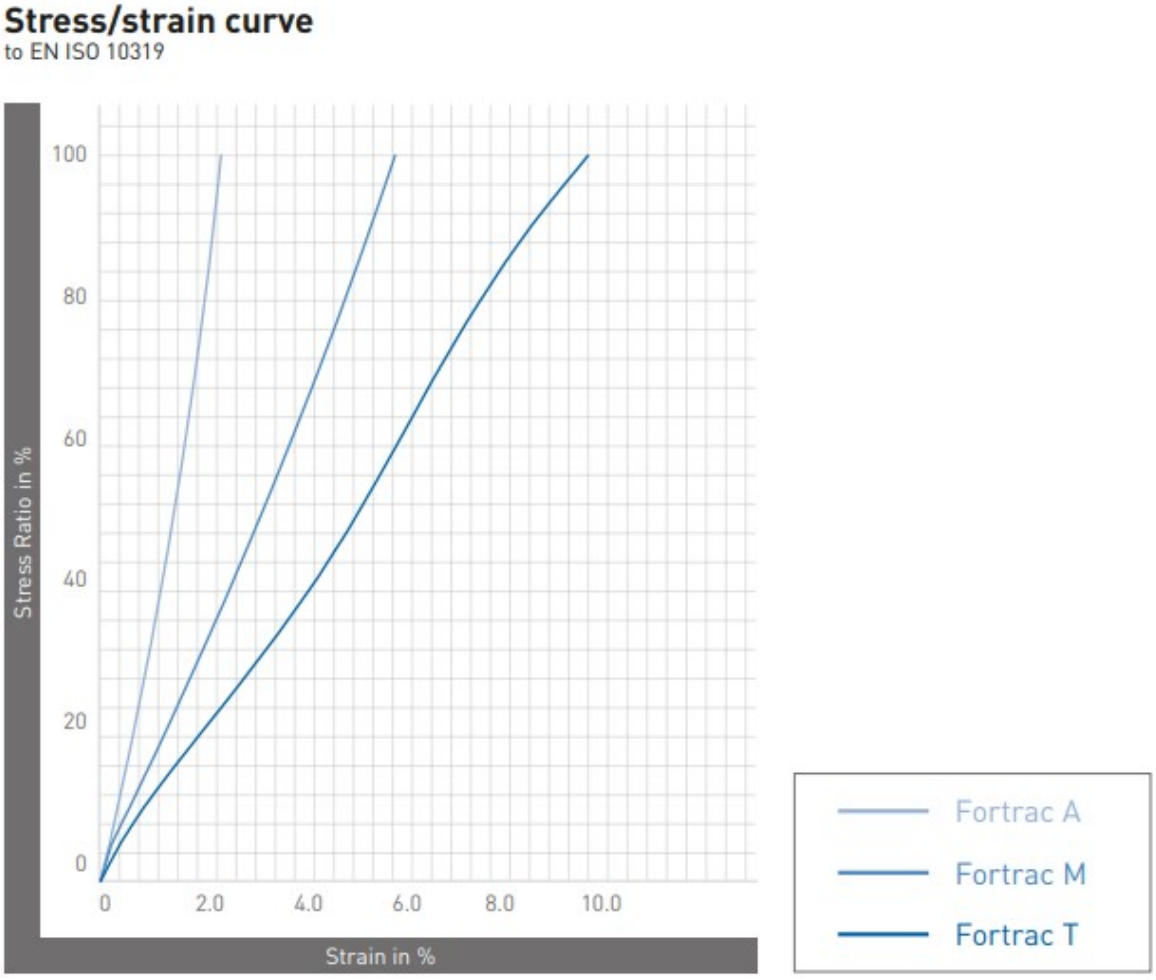

Figure 17 Stress strain-curve for Huesker Fortrac geogrids.

3.3.2.4 Facing

The facing is modelled as reinforced shotcrete with a thickness of, b = 18.5 mm. The stiffness parameters used are derived from a shotcrete with E = 39 GPa (Nilsson, 2003). Normal stiffness EA per meter is calculated as:

$$EA = E * b \tag{18}$$

And flexural rigidity as:

$$EI = E * \frac{h * b^3}{12} \quad (19)$$

Table 5 Properties of plate elements (facing)

Parameter	Name	Value	Unit
Material model	Model	Elastic	-
Normal stiffness	EA	720000	[kN/m]
Flexural Rigidity	EI	10	[kNm²/m]

3.3.3 Calculations

Four calculation sequences are performed in total. Two of the calculation sequences are performed with geosynthetic reinforcement with T_{ult} which is equal to $T_{\text{req,gov}}$ for the end of construction stage. Surcharge loads are then applied in steps until the calculation cannot be completed at which point the wall is assumed to have reached failure.

Two calculation sequences are performed with T_{ult} which is lower than $T_{\text{req,gov}}$ for the end of construction phase. No further calculation stages are performed in these sequences.

Table 6 Calculation sequence 1, staged construction for $\boldsymbol{T_{\text{ult}} = 11\ kN/m}$ and $\boldsymbol{S_{\text{v}} = 0.5m}$

Stage	Calculation type	Explanation
1	K0 procedure	Generates initial stresses
2-10	Plastic	Calculates elastic-plastic deformations during construction of the GRS-wall in stages of 1.0 m
11	Plastic	End of construction
12	Plastic	Calculations with an evenly distributed load of 5 kPa
13	Plastic	Calculations with an evenly distributed load of 10 kPa
14	Plastic	Calculations with an evenly distributed load of 20 kPa
15	Plastic	Calculations with an evenly distributed load of 30 kPa
16	Plastic	Calculations with an evenly distributed load of 40 kPa
17	Plastic	Calculations with an evenly distributed load of 50 kPa. Last completed phase.

Table 7 Calculation sequence 2, $\boldsymbol{T_{\text{ult}} = 19\ kN/m}$ and $\boldsymbol{S_{\text{v}} = 1.0m}$

Stage	Calculation type	Explanation

1	K0 procedure	Generates initial stresses
2-5	Plastic	Calculates elastic-plastic deformations during construction of the GRS-wall in stages of 1,0 m
6	Plastic	End of construction.
7	Plastic	Calculations with an evenly distributed load of 5 kPa
8	Plastic	Calculations with an evenly distributed load of 10 kPa
9	Plastic	Calculations with an evenly distributed load of 20 kPa
10	Plastic	Calculations with an evenly distributed load of 30 kPa
11	Plastic	Calculations with an evenly distributed load of 35 kPa. Last completed phase.

To establish a mesh that is fine enough to produce reliable calculations, calculation sequence 1 was performed with increasingly finer mesh until convergence is satisfactory. The criteria used was that the difference in maximum total deformation in last the last calculation stage should be less than 1%. The first calculation was done with a medium mesh. The mesh was not refined for the soil present initially as deformations is mostly occurring in and near the reinforced zone of the model. Mesh density very fine was deemed sufficient.

4 Results

4.1 Required ultimate strength according to SGF (2004)

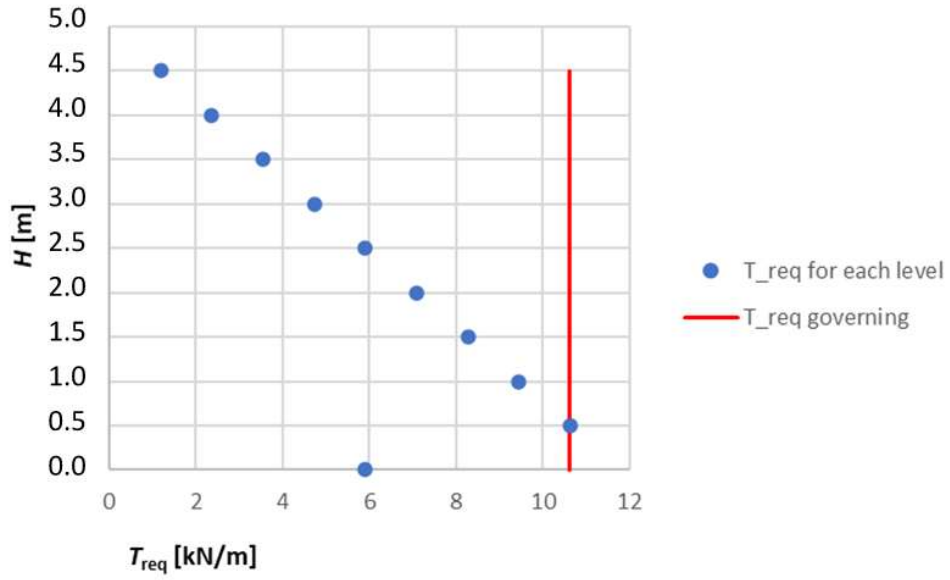

Figure 18. The figure shows the required tensile strengths for each reinforced level relative to the active earth pressure. The red line shows the governing tensile strength when a uniform geosynthetic layers is insertedas calculated by SGF (2004) .

In Figure 18 T_{req} is calculatedfor end of construction phase 1 for all reinforcement levels as calculated with SGF (2004). Figure 18 also shows $T_{\text{req,gov}}$, the required tensile strength if a uniform geosynthetic is used for the whole GRS-wall. As seen in the figure $T_{\text{req,gov}}$ occurs at H=0.5 m since the earth pressure is largest at this level

Table 11 and table 12 shows the required governing tensile strength $T_{\text{req,gov}}$ for all phases of calculation sequence 1 and sequence 2 respectively. The GRS-wall is at the limit of tensile overstress according to SGF (2004) at the end of construction phase. In the following surcharge load phases T_{ult} is insufficient against tensile overstress according to SGF (2004).

Table 11 Required tensile strength values, $\boldsymbol{T_{\text{req}}, gov}$ as calculated with SGF (2004) for calculation sequence 1, where $\boldsymbol{T_{\text{ult}} = 11\ kN/m}$.

Q [kN/m]	0	5	10	20	30	40	50
T_{req}, gov [kN/m]	10.63	11.25	11.87	13.11	14.36	15.60	16.84

Table 12 Required tensile strength values, $\boldsymbol{T_{\text{req}}}$ as calculated with SGF (2004) for calculation sequence 2, where $\boldsymbol{T_{\text{ult}} = 19\ kN/m}$.

Q [kN/m]	0	5	10	20	30	35
$T_{\text{req,gov}}$ [kN/m]	18.90	20.13	21.38	23.86	26.35	27.59

4.2 Results of FEM calculations

4.2.1 Calculation sequence 1 - end of construction stage

4.2.1.1 Horizontal earth pressure at end of construction

Figure 19 shows σ_h at the Rankine soil wedge as calculated with Plaxis and σ_a. As can be seen in the figure σ_h corresponds well with σ_a, as would be expected.

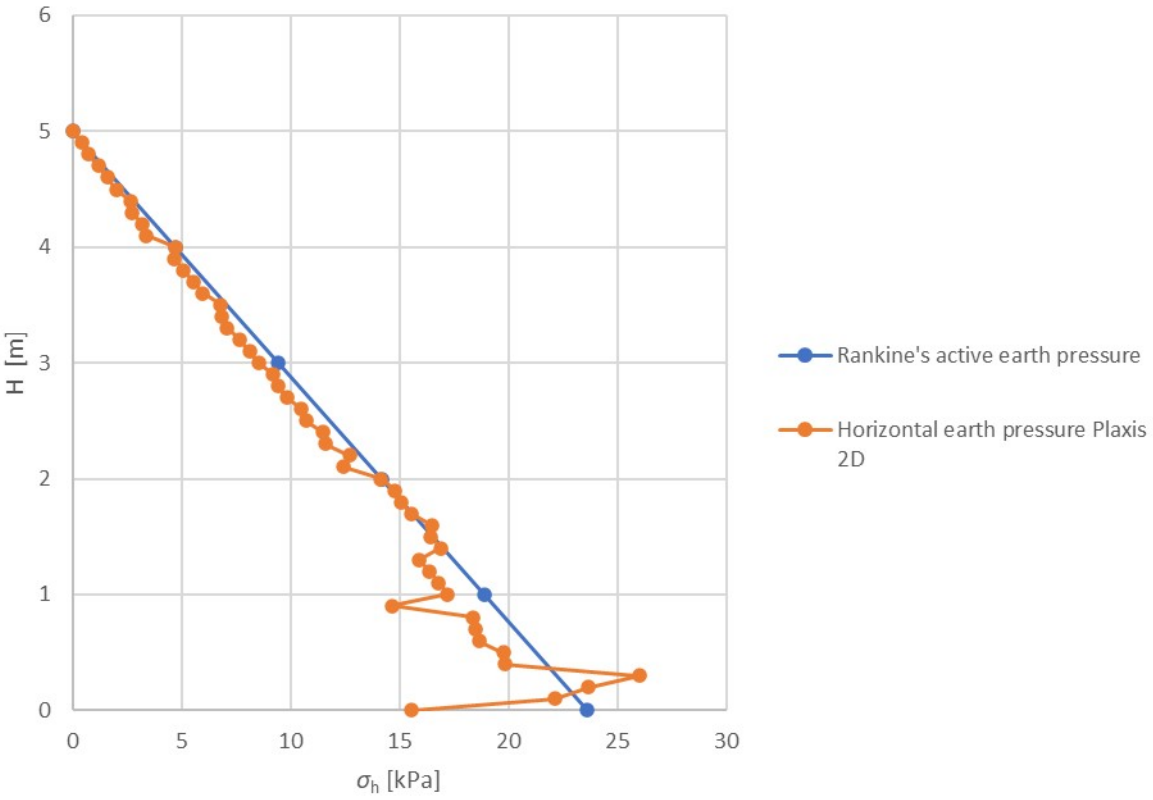

Figure 19 Rankine's active earth pressure and the horizontal earth pressure as calculated in calculation sequence 1 end of construction stage at the Rankine soil wedge.

4.2.1.2 *Mobilized tensile force and strain*

As seen in **Fel! Hittar inte referenskälla.**, most reinforcement levels show a maximum strain in the geogrid of up to 2 %, which is within acceptable at working stress conditions. The maximum strain in the bottom of the wall is close to zero which would mean that no or very little tensile stress is developed in the base reinforcement layer and the highest values around mid hight. The distribution of T_{mob} between the geogrids approximately follows SGF (2004), except the peak for T_{mob} occurs at H=1 m instead of H=0.5 m. The mobilization is significantly lower than T_{req} as M at H=1.0 is only 0.67 and 0.61 at H=0.5. T_{req} at these levels are 0.85 and 1.0, respectively. This means that there is a slight difference in the distribution between the geogrids and a quite large difference in the development of tensile force between the FEM-calculation and the analytical calculation from SGF (2004). Looking at T_{mob} in **Fel! Hittar inte referenskälla.**, which shows the mobilized force at the expected peak around the Rankine soil wedge, the forces in the geogrid appears to wear off at higher levels in the wall. Looking at Figure 20, however paints a different picture. The forces along the soil wedge follow the trend of the T_{req} approximately but the forces at the facing interface are quite uniformly distributed and only slightly lower than $T_{mob,max}$.

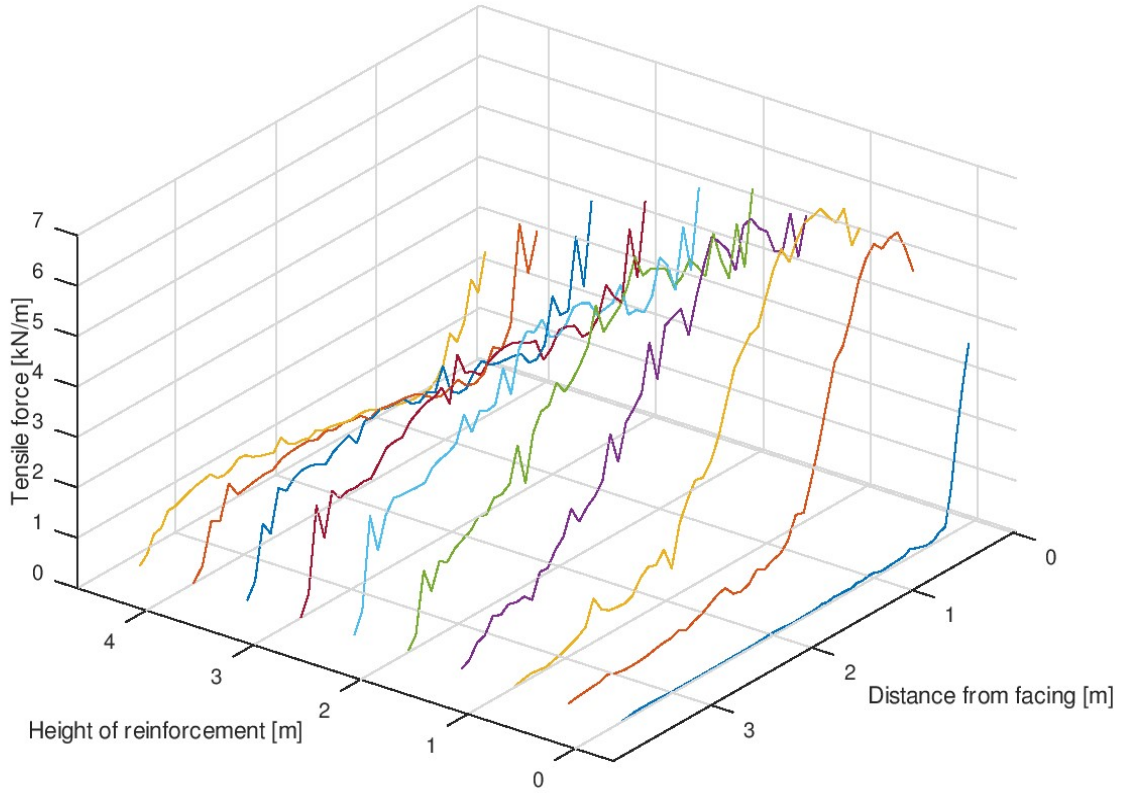

Figure 20 Distribution of tensile force in the reinforcements for each level at end of construction for calculation sequence 1

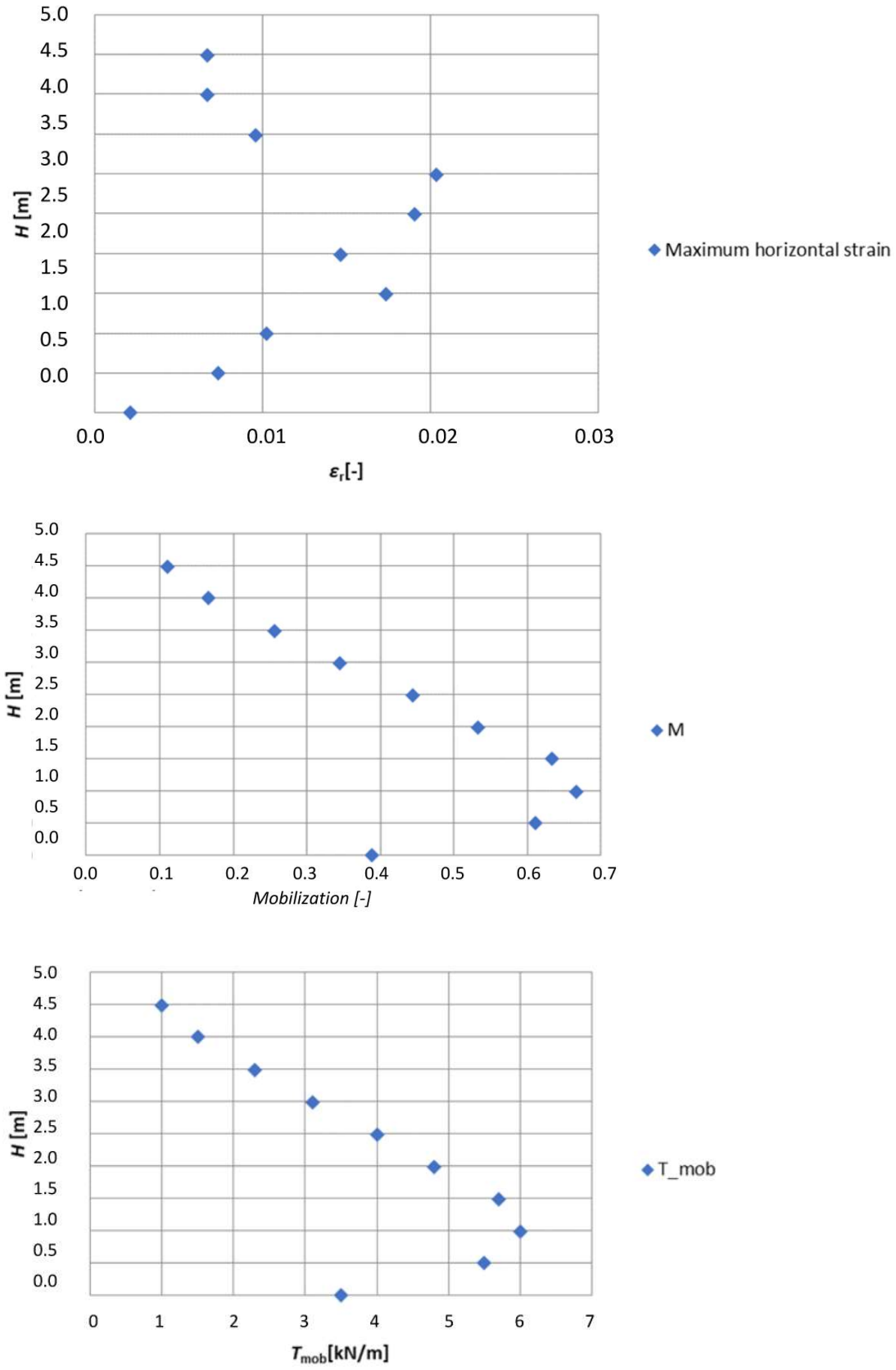

Figure 21 $\boldsymbol{\varepsilon_r}$, T_{mob} and M for the end of construction stage of calculation sequence 1

4.2.1.3 Toe restraint

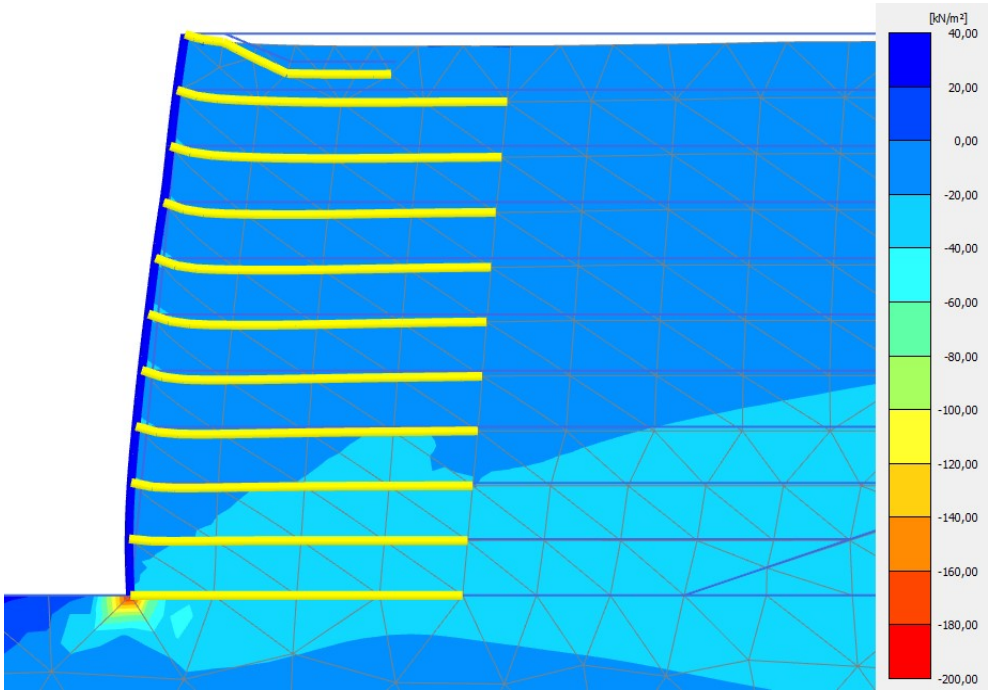

Figure 22 σ_h at the toe of the wall.

In Figure 22 we can see that there is a significant amount of horizontal pressure developing at the toe of the wall as it is restrained from moving outwards by the fixed point at the toe of the wall. The fixation of the toe together with the stiffness of the facing means that the lower part of the wall is more restrained from moving outwards which would cause the lower values of ε_r and in turn $T_{mob,}$ moving $T_{mob,max}$ up a one level compared to $T_{req,max}$ as seen in **Fel! Hittar inte referenskälla.**.

4.2.2 Calculation sequence 1 - load test

In this section the results of the surcharge loading in calculation sequence 1. The wall is surcharge loaded in stages with a uniformly distributed q = 5, 10, 20, 30, 40, and 55 kPa.

4.2.2.1 Mobilized tensile force and strain

As surcharge loads are applied ε_r and T_{mob} increases as expected, as seen in **Fel! Hittar inte referenskälla.**. The increases up to q = 10 kPa are quite small, but at q = 20 kPa a shift happens where ε_r suddenly becomes larger. The same pattern can be observed for T_{mob}, but only for H=0.5, 1.0 and 1.5 m. At q = 30 kPa the geogrids above can also be observed to have increased their tension which makes the loading distribution more equal between the geogrids. The loading can continue up to 55 kPa after which the simulation fails due to soil body collapse. At q=50 kPa the geogrid at H=0.5 m reaches M=0.99 at q=55 kPa the geogrids at H=0.5, 1.0, 1.5 and 2.0 m are fully mobilized with M=1.0 and ε_r=0.1 to 0.12.

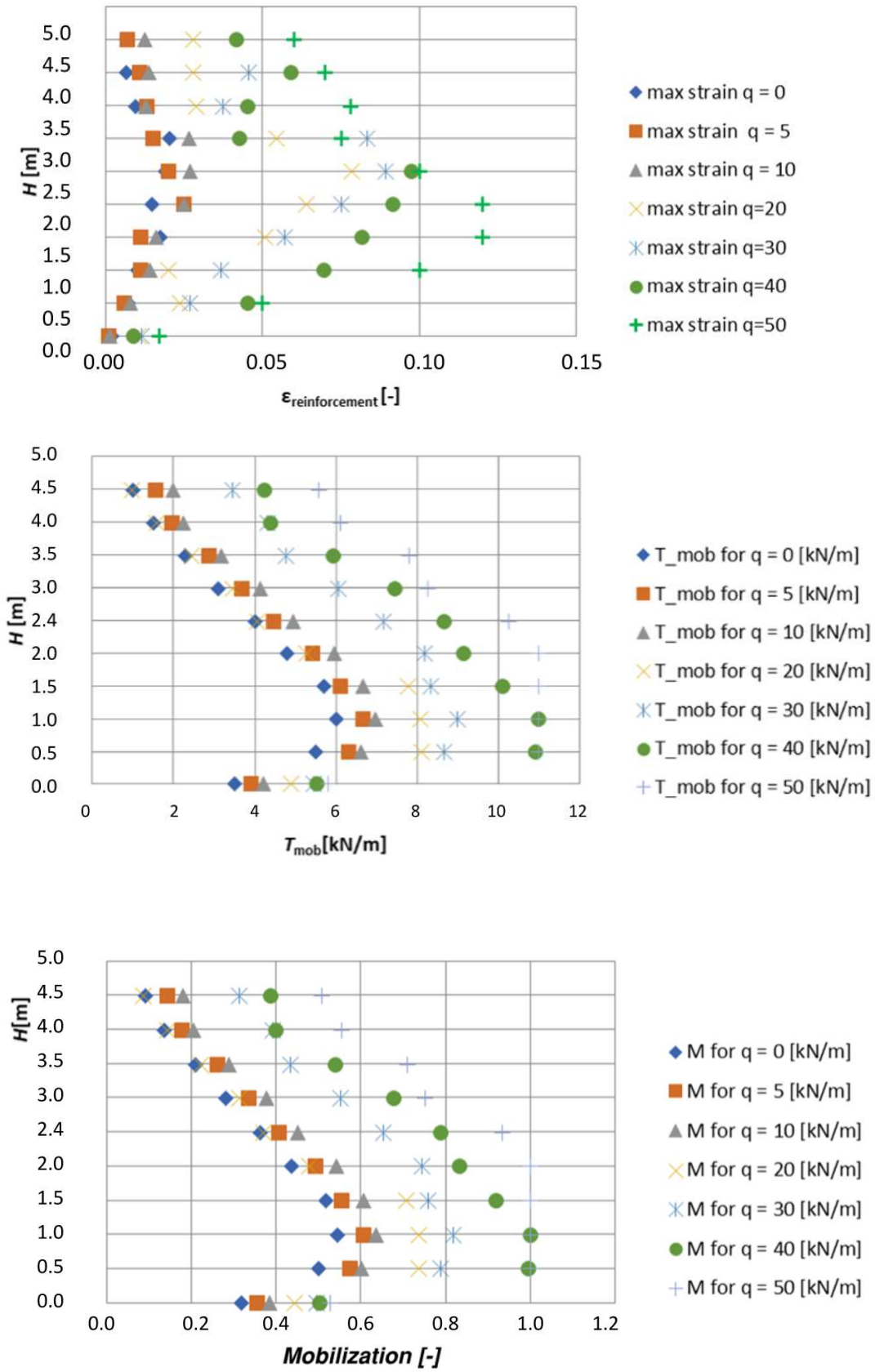

Figure 24. Strain, Mobilized force and degree of mobilization for calculation sequence 1.

4.2.2.2 Wall deformations

As the GRS-wall is surcharge loaded the facing starts to bulge outwards as can be seen in Figure 23. With the biggest movements occurring at the lower third of the wall which is to be expected as the biggest strains and loads in the geogrids are observed here as seen in **Fel! Hittar inte referenskälla.**.

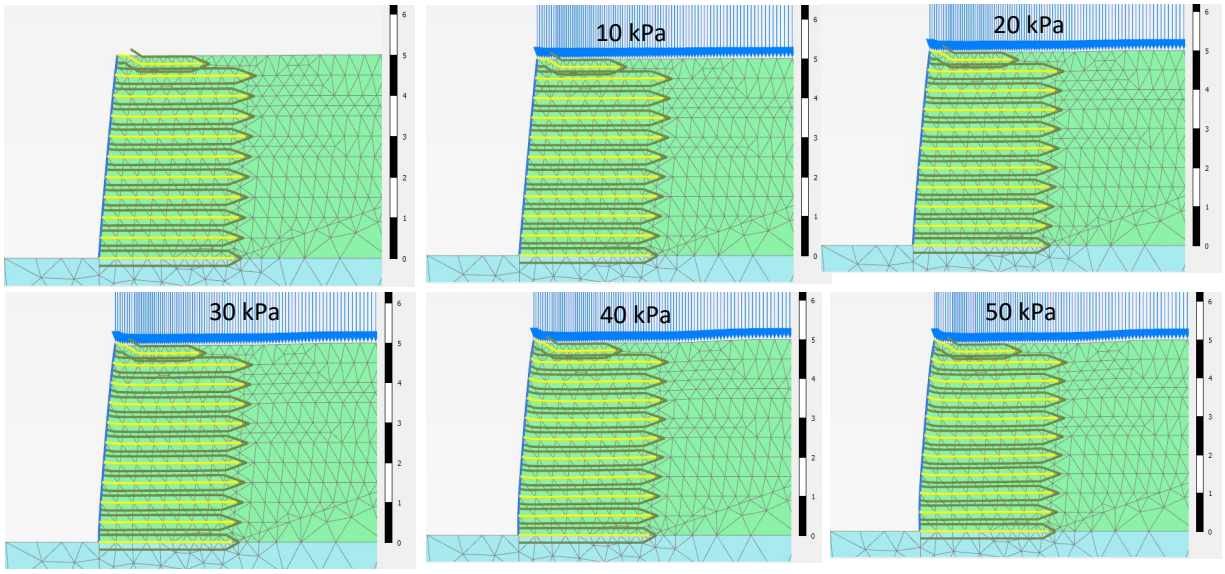

Figure 23 Wall movements displayed with deformed mesh at true scale for calculation sequence 1

In **Fel! Hittar inte referenskälla.** horizontal movements six nodes are shown. The horizontal movements are the biggest approximately at mid height where the highest strains are observed in **Fel! Hittar inte referenskälla.** Horizontal movement at the toe of the wall is very small. Horizontal movements at the crest of the wall and at the top 2.5 m behind the crest are approximately the same. Horizontal movements at the top 5 m behind the crest is much smaller than the movements at the crest. At the top 10 m behind the crest there is no horizontal movement at all.

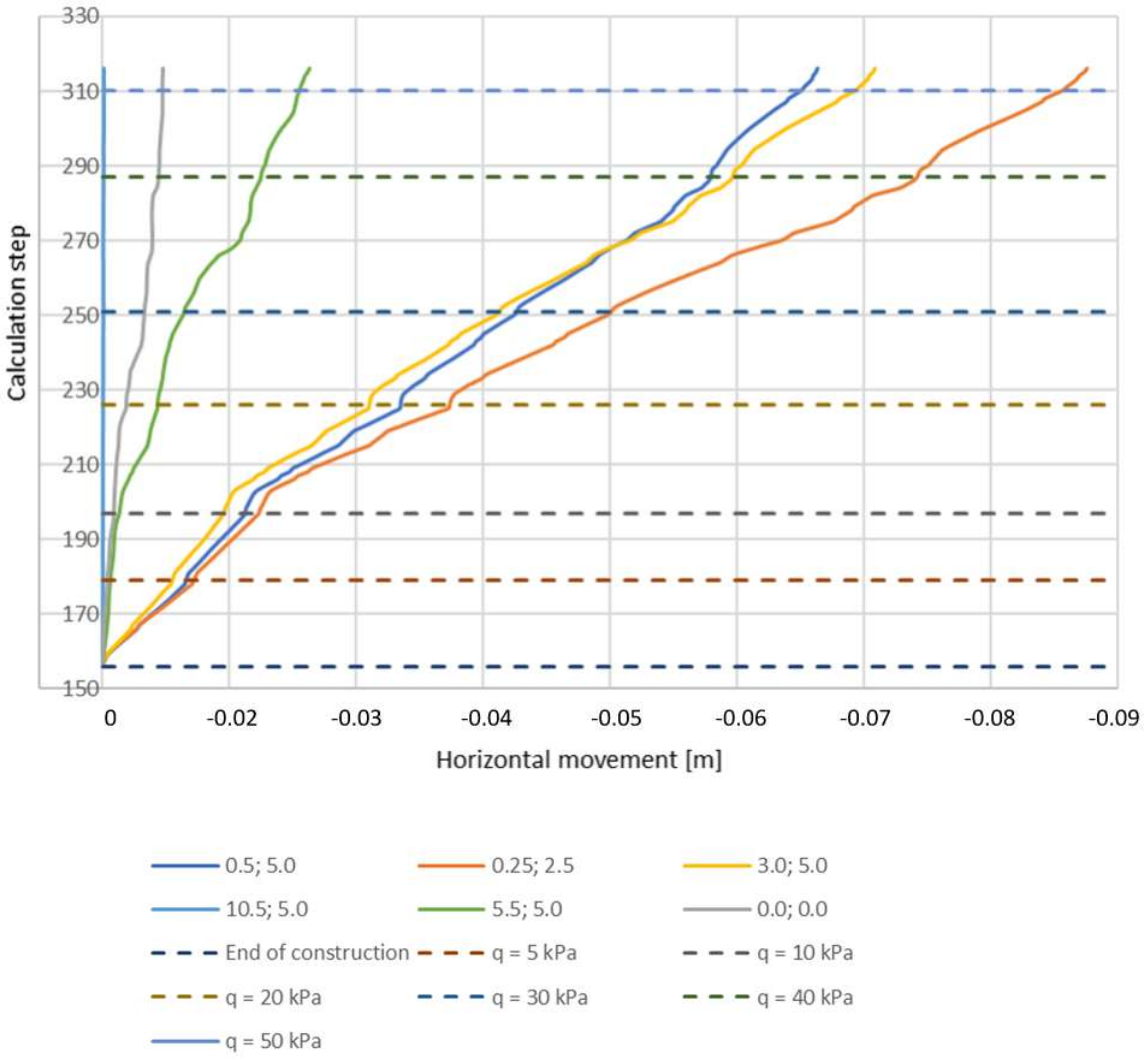

Figure 24 Horizontal movement of calculation nodes in solid lines. Nodes are named after their cartesian coordinate in meters with origo at the toe of the GRS-wall. Dotted lines mark the calculation stage.

4.2.3 Calculation sequence 2 - Wider reinforcement spacing

4.2.3.1 Mobilized tensile force and strain

In **Fel! Hittar inte referenskälla.**, the maximum strains for each reinforcement level and calculation stage for calculation sequence 2. The results from the calculations show quite similar strains for the unloaded stage and the first surcharge load stages. At the final load stage the strains suddenly becomes a lot larger indicating that the geogrids are starting to plasticize.

As the loading progresses to higher surcharge loads the tensile forces in the reinforcements increases at all levels, with higher degree of mobilization one can however observe that the distribution becomes a bit more uniform across among the reinforcements in the middle of the wall at the later load stages. Compared to calculation sequence 1, calculation sequence 2 displays a similar pattern as the simulation fails as full mobilization of the geogrids occur as M almost reaches 1 at H=0.5 and 2.0 m. ε_r is also approximately in the same range with the last loading stage recording a peak value of ε_r=0.12.

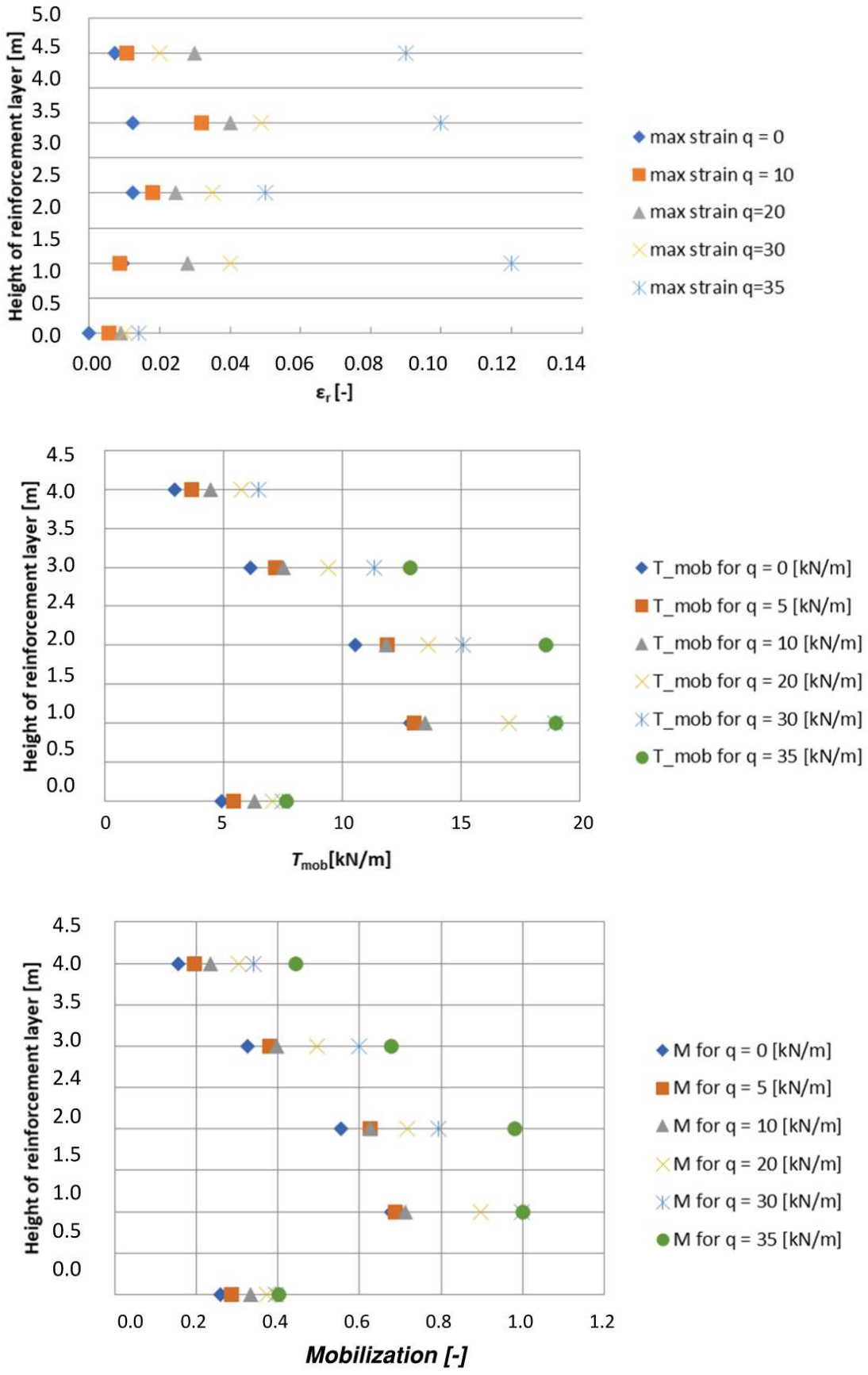

Figure 25. Strain ε_r, Mobilized force T_{mob} and degree of mobilization M for calculation sequence 2

5 Discussion and conclusions

5.1 Summary

The result of the numerical model is elaborated, and a comparison is made between the limit equilibrium model and the Finite element model of the GRS-wall, both in ultimate limit state (ULS) and serviceability limit state (SLS).

The LEM-model is the benchmark model since it is the standard model in practical design. The limit equilibrium mechanism in this model is the earth pressure distribution which is resisted by the geosynthetic reinforcement. As Figure 18 shows, the maximum tensile load occurs at the base of the GRS-wall where the active earth pressure is largest is a uniform geosynthetic reinforcement is used. The LEM model does not include the deformations of the soil and the geosynthetic layers, and the redistribution of load between the geosynthetic layers as the mobilization factor increases.

The finite element model includes the active earth pressure through the Mohr-Coulomb yield criteria, in which the active earth pressure is occurring along the expected line of the Rankine soil wedge in the numerical model. The load effect which is resisted by the bearing capacity of the geosynthetic reinforcement is consequently the same as in the limit equilibrium model.

There are however some differences between the limit equilibrium and finite element models. T_{req} does however not correspond with T_{mob} in the finite element modelwith T_{mob} being significantly lower than T_{req} and approximately trapezoidal distribution of the loads rather than the triangular distribution assumed by SGF (2004). This means that there are other factors determining the tension in the geogrid other than just the horizontal earth pressure applied strictly to the geogrids.

The load distribution along the geosynthetic reinforcements is also different in the finite element model compared to the limit equilibrium model. A load redistribution occurs in between the geogrids when they are mobilized, mainly in the lower part of the construction where the loads are the highest. The load distribution becomes more pronounced as the wall is incrementally surcharge loaded to failure. At last load stage the geogrids reach yield for geogrids levels up to 2.0 m. This occurs for the wall with both Sv=0.5 and Sv =1.0 m.

The wall with Sv = 1.0 and T = 19 kN/m could be load with a distributed load up to 35 kPa before soil body collapse of the simulation, whereas the wall with Sv = 0.5 and T = 11 kN/m could be surcharge loaded up to 50 kN kPa even though they have the same design capacity according to the SGF (2004).

The finite element model could therefore be loaded to a significantly higher surcharge load compared to the limit equilibrium model, which has reached maximum capacity before any surcharge load was placed on the GRS-wall. The ultimate limit state bearing capacity in the finite element model was therefore larger.

The serviceability limit state is not calculated in the limit equilibrium model, but the standard design method with maximum Sv = 0.5 is considered to results in small deformations.

The finite element model can calculate the deformations at different mobilization ratios of the geosynthetic reinforcement. The strains in the geogrids are in the acceptable range 1-2% at the first loading stage (without surcharge load) defined as the ULS of SGF (2004). This indicates that no further measures need to be taken to ensure that unacceptable movements would occur when designing a wall of this configuration according to TK Geo 13 (Trafikverket 2014).

The max strains in the geogrids calculated with the finite element model at full mobilization are 9-12% which is roughly equal to the stress-strain relationship of a Fortrac T geogrid, which is 10 % according

to the manufacturer's specification. The stress-strain relationship of the constitutive model used in the simulations appear to replicate the behaviour of the real geogrid well in this regard.

There is an influence on the mobilization of tension in the geogrids from the facing and the toe, as the distribution of T over the length of the geogrid does not consequentially peak at the yield surface of the Rankine soil wedge as assumed by SGF (2004). The distribution of T has a second peak at the facing, which for some levels is larger than the peak at the yield surface of the soil wedge. The sum of T_{mob} is less than the P_a which means that the structure is not at static equilibrium if one does not account for loads being taken up by some other part of the structure other than the load taken by the geogrid at the soil wedge.

5.2 Conclusions

The FEM calculations carried out for this thesis shows that active earth pressure occurs at the Rankine soil wedge, as assumed in SGF (2004) meaning the assumption of active earth pressure is justified. It does however not mean that all that pressure is transferred into the geogrids as the design method would assume. At low levels of mobilization in the reinforcements the tensile force in the reinforcements is increasing linearly with the depth in the structure. At higher levels of mobilization, i.e., when the reinforcements are closer to or at their ultimate strength the load is redistributed to nearby reinforcements. The redistribution of loads creates a ductile failure rather than the brittle failure assumed in SGF (2004). Load is also carried by the facing and transferred through the toe to the ground. This also means that the load bearing capacity is larger than expected. The design criteria for internal stability in SGF (2004) is therefore on the conservative side when compared to the numerical calculations.

Load is distributed between the geogrids. In the simulation the soil collapses as geogrids in the range of 2 m from each ot Spacing between the geogrids does not seem to influence the distribution, at least for the range of S_v recommended in SGF (2004) for the specific parameters used in this study. The potential for redistribution of load between the geogrids means there is some redundancy in the reinforcement as compared to the design method of SGF (2004). The study suggests that the capacity of the GRS-wall for surcharge loads as designed with SGF (2004) is a lot higher than the design method predicts.

The stiffness of the facing and friction or fixation of the toe can influence the distribution of T along the geogrid. To what extent this is the case cannot be concluded, as there is no variation of EI for the facing done in this study. As high tension is observed in the geogrid-facing interface, load is transferred to the facing which demands sufficient connection strength and strength of the facing itself. A less stiff facing would likely lead to a larger utilization of the geogrid as reinforcement for the same loading conditions. Conversely a stiff facing may render the geogrids not fully utilized as designed as load is transferred to the facing. A potential pit fall of this is that there is no method in SGF (2004) for determining the design connection or facing strength. A stiff but weak facing may lead to bulging of the facing element or failure as the stiff facing element takes part of the load from the horizontal earth pressure.

The constitutive models of the geogrids in Plaxis 2D, elastic and elastic-plastic, lacks a distinct failure criterium. The elastic-plastic model, which is used in the study, determines the yield strength at a specified load at which point the material deforms plastically. When using the elastic-plastic constitutive model it is reasonable to assume that the yield point of the geogrid is equal to failure even though it does not mark the ultimate failure of the material, as there is still a residual strength in the geogrid after this point. As seen in the simulations, the maximum strains before the reinforcements are fully mobilized, ie. at the point of yield, the strains are in the working range for normal geogrid materials. The calculation stage for each sequence when geogrids are fully mobilized are the last of each sequence before the next stage, where the calculations cannot be completed due to soil body

collapse. This might be viewed as a sort of residual strength of the structure, which could be expected as the geogrid, both the constitutive model and the real material have a ductile failure mode.

The results of the FEM calculations show a similar distribution to the distribution suggested in (Zornberg, et al., 1998). This study does not attempt to answer the question regarding the extent of the redistributing capacity of geosynthetic. The reinforcements of the modelled GRS-walls reached full full mobilization from the base up to less than half of the height of the wall (2 m) at the last successful loading stages for each scenario. There is no apparent significant difference between the redistribution capacity for walls with different spacing width between the reinforcement layers, as the distribution of mobilized tensile force for the wall with $S_v = 0.5$m and $S_v = 1.0$m were approximately the same. There could possibly be an effect with more load redistribution for even smaller spacing widths and less load redistribution for larger spacing widths. Effects on the redistribution from the length the reinforcements was not examined, the length was however set to $0.7*H$ which is in the middle range for suggested reinforcement lengths in SGF (2004). The possible effect of varying soil parameters on the load redistribution is also not possible to conclude from this study, as is the effect of facing stiffness, basal friction and toe restraint.

There is no physical testing done to validate the findings of this study, there have however been several studies which have validated numerical studies with measured mechanical behaviour (Hatami & Bathurst, 2005) (Reddy, et al., 2003) (Allen & Bathurst, 2002). This study has used verified methods of simulating the structural behaviour and the findings of this study corresponds well with prior studies, both physical and numerical.

5.3 Recommendations

There are several parameters that are not studied which might influence how the GRS-wall behaves. From this study the stiffness of the facing appears to be relevant in determining the load distribution, but as the stiffness is not varied it cannot be determined in what way the load distribution would change with a stiffer or less stiff configuration. Other parameters which could be important to study is the friction angle of the soil, the length of the geogrids, base friction and toe restraint.

For normal applications with simple geometry, simple loading conditions and moderate wall height the (SGF, 2004) should be sufficient in designing reliable GRS-walls as long as care is taken to the design of the facing. The use of advanced software such as Plaxis 2D is probably best reserved for more complicated designs as even a simple design is quite laborious and sensitive to the movements which occur. In designs with more complex geometry FEM-modelling can be useful as SGF (2004) does not offer a design method for such cases.

References

Allen, T. M. & Bathurst, R. J., 2002. Soil reinforcement loads in geosynthetic walls at working stress conditions. *Geosynthetics international,* 9(5-6), pp. 525-566.

Allen, T. M., Bathurst, R. J. & Berg, R. R., 2002. Global level of safety and performance of geosythetic walls: An historical Perspective. *Geosynthetics International,* 9(5-6), pp. 359-450.

Bathurst, R. J. & Benjamin, D. J., 1990. Failure of geogrid-reinforced soil wall. *Transportation Research Record Journal of the Transportation Research Board*, Jan, pp. 109-116.

Bathurst, R. J. & Simac, M. R., 1994. *Geosynthetic Reinforced Segmental Retaining Wall Structures in North America.* Singapore, s.n.

Bathurst, R. J. et al., 2006. The influence of facing stiffness on the performance of two geosynthetic reinforced soil retain walls. *Canadian Geotechnical Journal,* Issue 43, pp. 1225-1237.

Bendzovski, R. & Melin, D., 2007. *Analys av dimensioneringsmetoder för stödkonstruktioner med polymerbaserad jordarmering,* Göteborg: Chalmers Tekniska Högskola.

Bilgin, Ö., 2009. Failure Mechanisms Governing Reinforcement Failure Length of Geogrid Reinforced Soil. *Engineering Structures,* Volume 31, pp. 1967-1975.

BSI, 1995. *Code of practice for strengthened/reinforced soils and other fills.* s.l.:BSI.

Carlsson, B., 1987. *Armerad jord beräkningsprinciper för vertikala väggar, branta slänter, bankar på lös undergrund, bankar på pålar,* s.l.: Terrateam AB.

Chen, W.-F., 1997. *Handbook of Structural Engineering.* 1st ed. Boca Raton: CRC Press.

CEN, 2021. Eurocode 7: Geotechnical design - part 3: Geotechnical structures. *prEN 1997-3,* CEN

Dobie, M. J. D. & McCombie, P. F., 2015. *Reinforced soil design using a two-part wedge mechanism: justification and evidence.* Edinburgh, ICE publishing.

German Geotechnical Society, 2011. *Recommendations for Design and Analysis of Structures using Geosynthetic Reinforcements - EBGEO.* 2nd ed. Berlin: Wilhelm Ernst & Sohn.

Guler, E., Demirkan, M. M. & Hamderi, M., 2007. Numerical analysis of reinforced soil-retaining wall structures with cohesive and granular back fills. *Geosynthetics international,* 14(6), pp. 330-345.

Hatami, K. & Bathurst, R. J., 2005. Development and verification of a numerical model for the analysis of geosynthetic-reinforced soil segmental walls under working stress conditions. *Canadian Geotechnical Journal,* Volume 42, pp. 1066-1085.

Heerten, C., 2012. Reduction of climate-damaging gases in geotechnical engineering practice using geosynthetics. *Geotextiles and Geomembranes*, Feb, Volume 30, pp. 43-49.

Helwany, S. M. B., Wu, J. T. H. & Froessl, B., 2003. GRS bridge abutments - an effective means to alleviate bridge approach settlement. *Geotextiles and Geomembranes,* 21(2003), p. 177–196.

Hoffman, P., 2015. *Plasticity and the mechanics of reinforced soil.* 1st ed. Denver: Preservation Engineering

Holtz, R. D., 2017. 46th Terzaghi lecture: geosynthetic reinforced soil: from the experimental to the familiar. Journal of Geotechnical and Geoenvironmental Engineering, 143(9)

Huang, B., Bathurst, R. J. & Hatami, K., 2009. Numerical Study of Reinforced Soil Segmental Walls Using Three Different Constitutive Soil Models. *Journal of Geotechnical and Geoenvironmental Engineering,* 135(10), pp. 1486-1498.

Huang, B., Bathurst, R. J., Hatami, K. & Allen, T. M., 2009. Influence of toe restraint on reinforced soil segmental walls. *Canadian Geotechnical Journal,* Volume 47, pp. 885-904.

Jaky, J., 1948. Pressure in silos. *Proc. 2nd ICSM,* Volume 1, pp. 103-107.

Jewell, R. A., 1996. *Soil reinforcement with geotextiles.* 1st ed. London: CIRIA.

Koerner, R. M., 2017. *Geosynthetic Reinforced Walls: Overview, Failures and Items for Approval ,* s.l.: ISSMGE.

Koerner, R. M. & Song, T. Y., 2001. Geosynthetic reinforced segmental retaining walls. *Geotextiles and Geomembranes*, 24 May, Issue 19, pp. 359-386.

Leschinsky, D., 2009. On Global Equilibrium in Design of Geosynthetic Reinforced Walls. *Journal of geotechnical and geoenvironmental engineering,* 135(3), pp. 309-315.

Nilsson, U., 2003. *Bearing capacity of fibre reinfoirced sprayed concrete anchored in rock,* Stockholm: Swedish rock engineering research.

Nordic Geosynthetic Group, 2005. *Nordic guidelines for reinforced soil.* 2nd ed. s.l.:The Nordic Geotechnical Socites Nordic Industrial Fund.

NorGeoSpec, 2017. *https://www.norgeospec.org.* [Online].

Owen, D. R. J. & Hinton, E., 1977. *Finite Element Programming.* Droitwich: AW Billit.

Rankine, W., 1857. On the stability of loose earth. *Philosophical Transactions of the Royal Society of London,* Volume Vol. 147.

Reddy, D. V. et al., 2003. *Long-term behaviour of geosynthetic reinforced mechanically stabilized earth (MSE) wall system - numerical/analytical studies, full scale field testing and design software development,* Boca Raton: Florida Department of Transportation .

SGF, 2004. *Armerad jord och fyllning, Nordisk vägledning.* Linköping: rapport 2:2004, Unitryck 2004.

Shukla, S., Sivakugan, N. & Das, B., 2011. A state-of-the-art review of geosynthetic-reinforced slopes. *International Journal of Geotechnical Engineering,* 5(1), pp. 17-23.

Statens Vegvesen, 2005. *Håndbok 016, Geoteknikk i vegbygging, armert jord,* s.l.: s.n.

Sällfors, G., 2001. *Geoteknik, jordmateriallära - jordmekanik.* Göteborg: Vasastadens bokbinderi.

Terzaghi, K. & Peck, R. B., 1948. *Soil mechanics in engineering practice.* 1st ed. NewYork: Wiley & Sons.

Trafikverket, 2014. *Trafikverketrs tekniska krav för geokonstruktioner TKGeo 13,* 2014: Trafikverket.

Trafikverket, 2014. *Trafikverketrs tekniska råd för geokonstruktioner TRGeo 13,* 2014: Trafikverket.

Wu, J. T. H., 2007. *Lateral earth pressure against facing of segmental GRS walls.* Denver, ASCE.

Wu, J. T. H., Pham, T. Q. & Adams, M. T., 2013. *Composite Behavior of Geosynthetic Reinforced Soil Mass,* Georgetown: Federal Highway Administration.

Xie, Y., Leschschinsky, B. & Yang, S., 2016. Evaluating reinforcement loading within surcharged segmental block reinforced soil walls using a limit state framework. *Geotextiles and Geomembranes,* Volume 44, pp. 831-844.

Zornberg, J. G. & Leshchinsky, D., 2003. Comparison of international design criteria for geosynthetic reinforced soil structures. *Landmarks in Earth Reinforcement,* Volume 2, pp. 1095-1106.

Zornberg, J. G. & Leshchinsky, D., 2003. Comparison of International Design Criteria for Geosynthetic Reinforced Structures. *Landmarks in Earth Reinforcement,* Volume 2, pp. 1095-1106.

Zornberg, J. G., Sitar, N. & Mitchell, J. K., 1998. Performance of geosynthetic reinforced slopes at failure. *Journal of geotechnical and geoenvironmental engineering,* 124(8), pp. 670-683.